Computer Assisted Mechanics and Engineering Sciences, 7: 251–277, 2000.

Gravity currents with temperature-dependent viscosity

John R. King, David S. Riley and Ahmos Sansom
Division of Theoretical Mechanics, School of Mathematical Sciences, University of Nottingham, Nottingham, NG7 2RD, U.K.

(Received September 13, 1999)

The spreading of fluid under gravity occurs in both nature and man-made situations and has been the subject of many previous studies. Considerably less attention has been paid to cases in which there is a strong thermal coupling influencing the flow. In this paper, simple models of the spreading of materials with temperature-dependent viscosity are presented and features that are commonly seen in experiments, such as plateauing and fingering, are shown to result. A model which includes latent heat effects is also briefly outlined.

1. Introduction

Despite its importance, the effect of cooling on the dynamics of a gravity current with a temperature dependent viscosity has not been extensively investigated; we start by reviewing briefly those studies of some relevance to the current work.

Experimental studies are more extensive than theoretical ones. In terms of the latter, two investigations should be mentioned. Sakimoto and Zuber [11] considered a variable viscosity material in developing a model of axisymmetric Venusian steep-sided or 'pancake' domes. Taking the eruption time of the hot dome material to be much smaller than the cooling and emplacement times, they assumed that spatial variability in the viscosity could be ignored and studied an analytically tractable problem in which the viscosity is assumed to have a power-law dependence on time. Their formulation is equivalent to a redefinition of time in the constant viscosity case (*cf.* Section 5.1.1 below) and cannot therefore lead to profiles that are steeper than the corresponding isothermal ones. At about the same time, Bercovici [3] developed a complementary model, also based on somewhat ad hoc modelling assumptions, but which incorporated radial variations. This investigation led to profiles exhibiting a plateau bounded by a steep flow front.

Early experimental work includes that performed by Fink and Griffiths [5] and [6] in which polyethylene glycol (PEG) was used to simulate lava flow. Warm liquid PEG, which is solid at room temperature and has a low melting point, was extruded into a cold bath of sucrose solution, forming a viscous gravity current. Depending on the flow rate and thermal conditions, the PEG surface solidifies and deforms through folding and fracturing processes.

In a similar experiment, Stasiuk *et al.* [15] investigated viscous gravity currents of warm glucose erupting radially at a constant rate into a tank filled with a cold aqueous solution. Their results showed quite beautifully the evolution of the vertical current profile away from the lens shapes predicted by the Barenblatt [2] similarity forms for the constant viscosity case (see Huppert [9]) and towards the steep fronted profiles characteristic of Venusian domes.

Snyder and Tait [14] studied experimentally the flow of laminar gravity currents intruding into a miscible, viscous ambient fluid. These exhibited fingering instabilities, for which two mechanisms were suggested, the first of which is gravitational: the no-slip condition on the substrate causes the nose of the current to lie some way above the substrate and to entrap buoyant ambient fluid. The second postulated mechanism relates to viscosity differences, being analogous to the Saffman–

Taylor finger instability observed when one fluid displaces a more viscous one in a Hele-Shaw cell (see Saffman and Taylor [10]).

A Bingham-type fluid (a PEG/kaolin slurry) was studied in Griffiths and Fink [7], experimental results revealing a much reduced sensitivity to the flow rate and thermal conditions compared to their earlier ([5] and [6]) PEG experiments, with the small bulbous 'pillows' that featured in the original experiments being replaced by lobes or spines.

The above studies were primarily motivated by geological applications. Another important motivation lies in safety studies of nuclear power plants. Plant operators are required to show that adequate safety margins exist even under severe accident conditions. This means that the relevant physical processes need to be sufficiently understood that corrective actions can be implemented effectively. For example, one extreme hypothetical situation is where it is supposed that the shutdown systems have failed to arrest some event that has led to the fuel in a particular channel overheating, causing the fuel inventory of that channel to melt and pour onto the floor below. In this application, the material generates internal heat as the radioactivity decays. As a contribution to such safety studies, Hallot *et al.* [8] carried out an experimental programme in which two different solidifying fluids, PEG and gum rosin, were extruded over a solid horizontal base (PEG features a sharp transition at the solidification temperature, whereas the properties of the rosin vary more gradually). The qualitative features of the PEG results were consistent with those found by Fink and Griffiths, described above. Hallot *et al.* also found, however, that there was a substantial contribution to the energy budget from an exothermic reaction between PEG and sucrose solution. Such internal energy sources therefore need to be considered when comparing experimental results with theoretical models; this does not seem to have been undertaken previously. Hallot *et al.* circumvented this complication by using ethylene glycol, which does not react with PEG, as the coolant and reported excellent agreement between their results from experiments and from scaling arguments.

We now outline the contents of the remainder of the paper. The low Reynolds number, small aspect ratio flows considered herein are assumed to be gravity-driven, the effects of surface tension forces being assumed to be negligible. The study is thus a natural development of the work of Huppert [9], who considered similarity solutions describing constant viscosity gravity currents from line and point sources.

Asymptotic analysis (lubrication theory) is first used to determine the evolution equation for the free surface, when the viscosity is dependent upon temperature, and the corresponding forms for the energy equation. For brevity, results are subsequently presented only for one constitutive law, an exponential viscosity temperature relationship. A number of different models are investigated. In the first, spreading of a fixed mass of fluid is considered when there is no internal heat generation and the boundaries are isothermal. In the second, a fixed mass of fluid is considered in an axisymmetric geometry and as it advects there is heat loss through cold boundaries but gain through internal heat generation. This model is extended to consider the effects of a constant rate of fluid injected from a point source. In the third model, a fixed mass of hot, poorly conducting fluid spreading axisymmetrically and losing heat through its cold boundaries is discussed. Finally, we consider the spreading of hot conducting fluid with constant mass which slowly loses heat through its boundaries. The model is initially considered in a two-dimensional Cartesian geometry and is then extended to a three-dimensional model of near-radial spreading.

The models are formulated in the next two sections. They are summarised in Section 4, where the boundary and initial conditions used in the numerical simulations are also briefly outlined; the results are presented in Section 5. Conclusions are discussed in Section 6; the Appendix details a related case involving basal solidification.

2. Derivation of the flow model

We consider a non-isothermal Newtonian fluid with temperature T and viscosity $\mu(T)$ spreading over a horizontal plane $z = 0$, (x, y, z) denoting a Cartesian coordinate system; see Fig. 1. The

equations governing the velocity $\boldsymbol{q} = (u, v, w)$ and pressure p (relative to atmospheric) are

$$\nabla \cdot \boldsymbol{q} = 0,$$

$$\rho\left(\frac{\partial \boldsymbol{q}}{\partial t} + (\boldsymbol{q}\cdot\nabla)\boldsymbol{q}\right) = -\nabla p + \nabla\cdot(\mu\nabla\boldsymbol{q}) + \frac{\mathrm{d}\mu}{\mathrm{d}T}\left[\nabla(\boldsymbol{q}\cdot\nabla T) - (\boldsymbol{q}\cdot\nabla)\nabla T\right] + \rho\boldsymbol{g},$$

where $\nabla = (\partial/\partial x, \partial/\partial y, \partial/\partial z)$, t is time, $\boldsymbol{g} = (0, 0, -g)$, g being the acceleration due to gravity, and ρ is density. All properties, except for the viscosity, are assumed constant. The free surface $z = h(x, y, t)$ is stress free while the substrate $z = 0$ is non-slip.

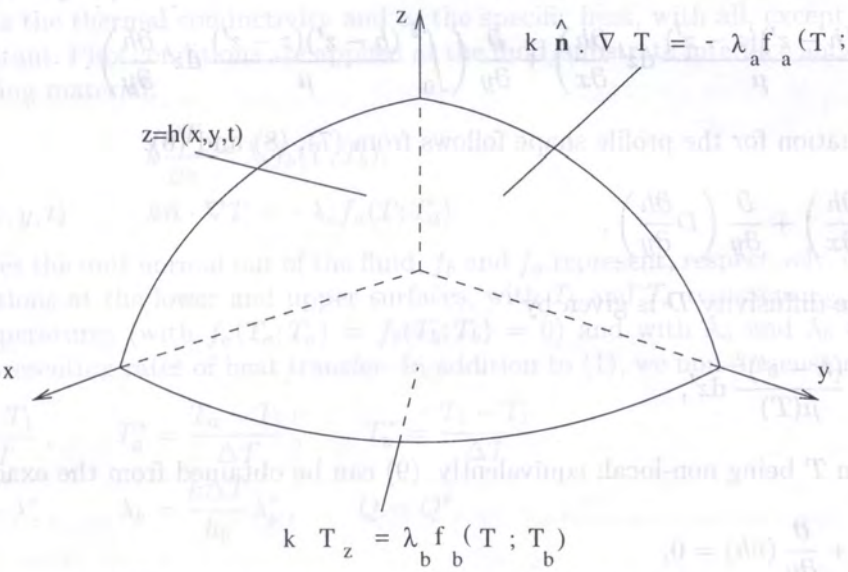

Fig. 1. Schematic of the geometry

We define the aspect ratio of the flow as $\epsilon = h_0/l_0$, where l_0 and h_0 are typical length scales in the horizontal and vertical direction directions, respectively. On taking characteristic viscosity and horizontal velocity scales as μ_0 and U_0, the equations are non-dimensionalised by introducing

$$x = l_0 x^*, \qquad y = l_0 y^*, \qquad z = h_0 z^*, \qquad u = U_0 u^*, \qquad v = U_0 v^*,$$
$$w = \epsilon U_0 w^*, \qquad \mu = \mu_0 \mu^*, \qquad t = \frac{l_0}{U_0} t^*, \qquad p = \frac{U_0 \mu_0 l_0}{h_0^2} p^*. \tag{1}$$

The above scales give rise to a Reynolds number $Re = \rho U_0 l_0/\mu_0$; we take $U_0 = \rho h_0^3 g/\mu_0 l_0$ to obtain a balance in the vertical momentum equation. In the limit $\epsilon \to 0$ with $Re = O(1)$ (or indeed $Re = o(\epsilon^{-2})$), the non-dimensional equations become:

$$\frac{\partial u}{\partial x} + \frac{\partial v}{\partial y} + \frac{\partial w}{\partial z} = 0, \tag{2}$$

$$-\frac{\partial p}{\partial x} + \frac{\partial}{\partial z}\left(\mu\frac{\partial u}{\partial z}\right) = 0, \tag{3}$$

$$-\frac{\partial p}{\partial y} + \frac{\partial}{\partial z}\left(\mu\frac{\partial v}{\partial z}\right) = 0, \tag{4}$$

$$-\frac{\partial p}{\partial z} - 1 = 0; \tag{5}$$

for clarity the stars have been dropped from the variables. Boundary conditions are

$$\text{at } z = 0 \qquad u = v = w = 0,$$
$$\text{at } z = h(x, y, t) \qquad \frac{\partial h}{\partial t} + u\frac{\partial h}{\partial x} + v\frac{\partial h}{\partial y} = w, \qquad \mu\frac{\partial u}{\partial z} = 0, \qquad \mu\frac{\partial v}{\partial z} = 0, \qquad p = 0. \tag{6}$$

The development of the evolution equation for the height profile follows from manipulating (2)–(6), subject to the above conditions. We thus have $p = h - z$ and the resulting horizontal velocity components are

$$u = -\int_0^z \frac{(h-z')}{\mu}\,\mathrm{d}z'\,\frac{\partial h}{\partial x}, \qquad v = -\int_0^z \frac{(h-z')}{\mu}\,\mathrm{d}z'\,\frac{\partial h}{\partial y}, \tag{7}$$

where in all such integrals μ denotes $\mu(T(x,y,z',t))$ (T being the dimensionless temperature defined below), whilst the vertical velocity is

$$w = \frac{\partial}{\partial x}\left(\int_0^z \frac{(h-z')(z-z')}{\mu}\,\mathrm{d}z'\,\frac{\partial h}{\partial x}\right) + \frac{\partial}{\partial y}\left(\int_0^z \frac{(h-z')(z-z')}{\mu}\,\mathrm{d}z'\,\frac{\partial h}{\partial y}\right). \tag{8}$$

The evolution equation for the profile shape follows from (7), (8) and (6):

$$\frac{\partial h}{\partial t} = \frac{\partial}{\partial x}\left(D\frac{\partial h}{\partial x}\right) + \frac{\partial}{\partial y}\left(D\frac{\partial h}{\partial y}\right), \tag{9}$$

where the effective diffusivity D is given by

$$D(h;T) = \int_0^h \frac{(h-z')^2}{\mu(T)}\,\mathrm{d}z', \tag{10}$$

the dependence on T being non-local; equivalently, (9) can be obtained from the exact result that

$$\frac{\partial h}{\partial t} + \frac{\partial}{\partial x}(\bar{u}h) + \frac{\partial}{\partial y}(\bar{v}h) = 0, \tag{11}$$

this being an expression of conservation of mass in which the vertically averaged velocity components are defined by

$$\bar{u} = \frac{1}{h}\int_0^h u\,\mathrm{d}z', \qquad \bar{v} = \frac{1}{h}\int_0^h v\,\mathrm{d}z', \tag{12}$$

so in the current case

$$\bar{u} = -\frac{1}{h}\int_0^h \frac{(h-z')^2}{\mu}\,\mathrm{d}z'\,\frac{\partial h}{\partial x}, \qquad \bar{v} = -\frac{1}{h}\int_0^h \frac{(h-z')^2}{\mu}\,\mathrm{d}z'\,\frac{\partial h}{\partial y}. \tag{13}$$

With regard to (10), it is instructive to rewrite the temperature in the form

$$T = T(x,y,\zeta,t), \qquad \zeta = z/h(x,y,t); \tag{14}$$

one then has

$$D(h;T) = h^3\int_0^1 \frac{(1-\zeta')^2}{\mu(T(x,y,\zeta',t))}\,\mathrm{d}\zeta'. \tag{15}$$

Although we have studied various constitutive laws for $\mu(T)$ (see Sansom [13]), only the widely adopted exponential law

$$\mu(T) = \exp(-\alpha T), \tag{16}$$

in which $\alpha \geq 0$ is a dimensionless constant and $T \geq 0$ is the dimensionless temperature, will be considered here.

3. Derivation of the thermal model

3.1. Formulation

The basic equation governing the temperature $T(x,y,z,t)$ is

$$\rho c_p\left(\frac{\partial T}{\partial t}+(\boldsymbol{q}\cdot\nabla)T\right)=\nabla\cdot(k\nabla T)+\upsilon Q,$$

where positive υQ represents a heat source term (Q being dimensionless and υ a dimensional constant), k is the thermal conductivity and c_p the specific heat, with all, except possibly Q, being assumed constant. Flux conditions are applied at the fluid/substrate interface and at the free surface of the spreading material:

$$\text{at } z=0 \qquad k\frac{\partial T}{\partial z}=\lambda_b f_b(T;T_b),$$

$$\text{at } z=h(x,y,t) \qquad k\hat{\boldsymbol{n}}\cdot\nabla T=-\lambda_a f_a(T;T_a).$$

Here $\hat{\boldsymbol{n}}$ denotes the unit normal out of the fluid, f_b and f_a represent, respectively, dimensionless heat transfer functions at the lower and upper surfaces, with T_b and T_a representing the corresponding external temperatures (with $f_a(T_a;T_a)=f_b(T_b;T_b)=0$) and with λ_a and λ_b being dimensional constants representing rates of heat transfer. In addition to (1), we non-dimensionalise according to

$$T^*=\frac{T-T_1}{\Delta T},\qquad T_a^*=\frac{T_a-T_1}{\Delta T},\qquad T_b^*=\frac{T_b-T_1}{\Delta T},$$

$$\lambda_a=\frac{k\Delta T}{h_0}\lambda_a^*,\qquad \lambda_b=\frac{k\Delta T}{h_0}\lambda_b^*,\qquad Q=Q^*,$$

$$\upsilon=\frac{k}{h_0^2}\upsilon^*,\qquad f_b(T;T_b)=f_b^*(T^*;T_b^*),\qquad f_a(T;T_a)=f_a^*(T^*;T_a^*),$$

leading to a Peclet number $Pe=\rho c_p U_0 l_0/k$. The temperature is thus measured relative to T_1 in units of ΔT, T_1 and ΔT being chosen in each sub-case in order to obtain the most convenient formulation.

Again dropping the stars, we thus have the dimensionless formulation

$$\epsilon^2 Pe\left(\frac{\partial T}{\partial t}+u\frac{\partial T}{\partial x}+v\frac{\partial T}{\partial y}+w\frac{\partial T}{\partial z}\right)=\frac{\partial^2 T}{\partial z^2}+\epsilon^2\left(\frac{\partial^2 T}{\partial x^2}+\frac{\partial^2 T}{\partial y^2}\right)+\upsilon Q,$$

$$\text{at } z=0 \qquad \frac{\partial T}{\partial z}=\lambda_b f_b(T;T_b), \tag{17}$$

$$\text{at } z=h(x,y,t) \qquad \frac{\partial T}{\partial z}-\epsilon^2\left(\frac{\partial h}{\partial x}\frac{\partial T}{\partial x}+\frac{\partial h}{\partial y}\frac{\partial T}{\partial y}\right)=-(1+\epsilon^2\nabla h\cdot\nabla h)^{\frac{1}{2}}\lambda_a f_a(T;T_a),$$

together with suitable initial and boundary data. In the above, Q, f_a and f_b are all be taken (by suitably defining υ, λ_a and λ_b) to be $O(1)$ as $\epsilon\to 0$. Two key parameter ranges arise for (17) in the 'thin-film' limit $\epsilon\to 0$; these encompass the full range of behaviour in that limit and are outlined in Sections 3.2–3.3. Further simplifications are of clear physical significance and are described in Section 3.4. We introduce $Pe_r=\epsilon^2 Pe$, the reduced Peclet number, and note as consequences of (17) that

$$\epsilon^2 Pe\left[\frac{\partial}{\partial t}\left(\int_0^h T\,\mathrm{d}z\right)+\frac{\partial}{\partial x}\left(\int_0^h uT\,\mathrm{d}z\right)+\frac{\partial}{\partial y}\left(\int_0^h vT\,\mathrm{d}z\right)\right]$$

$$=\epsilon^2\left[\frac{\partial}{\partial x}\left(\int_0^h\frac{\partial T}{\partial x}\,\mathrm{d}z\right)+\frac{\partial}{\partial y}\left(\int_0^h\frac{\partial T}{\partial y}\,\mathrm{d}z\right)\right]$$

$$-\left[(1+\epsilon^2\nabla h\cdot\nabla h)^{\frac{1}{2}}\lambda_a f_a(T_h;T_a)+\lambda_b f_b(T_0;T_b)\right]+\upsilon\int_0^h Q\,\mathrm{d}z, \tag{18}$$

where $T_h = T\,|_{z=h}$, $T_0 = T\,|_{z=0}$, and, if there is no input or removal of fluid,

$$\epsilon^2 Pe \frac{\mathrm{d}}{\mathrm{d}t}\int_{\Omega(t)} T\,\mathrm{d}V = -\lambda_a \int_{\Gamma_a(t)} f_a(T_h;T_a)\,\mathrm{d}S - \lambda_b \int_{\Gamma_b(t)} f_b(T_0;T_b)\,\mathrm{d}S + \upsilon \int_{\Omega(t)} Q\,\mathrm{d}V, \tag{19}$$

where $\Omega(t) \subset \mathrm{R}^3$ is the fluid domain, $\Gamma_a(t)$ is the free surface $z = h$ and $\Gamma_b(t)$ is the part of the substrate $z = 0$ that is covered by fluid.

3.2. Regime I: Conduction limited $Pe_r = O(1)$

This case corresponds to poorly conducting fluids (such as liquid waxes, which have Prandtl numbers, $Pe/Re = \mu_0 c_p/k$, of $O(10^4)$) having $Pe_r = O(1)$, the fullest balance then occurring when $\upsilon, \lambda_a, \lambda_b = O(1)$ also. To leading order the resulting thermal model is evidently then

$$Pe_r\left(\frac{\partial T}{\partial t} + u\frac{\partial T}{\partial x} + v\frac{\partial T}{\partial y} + w\frac{\partial T}{\partial z}\right) = \frac{\partial^2 T}{\partial z^2} + \upsilon Q\,,$$

$$\begin{aligned} &\text{at } z = 0 && \frac{\partial T}{\partial z} = \lambda_b f_b(T;T_b), \\ &\text{at } z = h(x,y,t) && \frac{\partial T}{\partial z} = -\lambda_a f_a(T;T_a), \end{aligned} \tag{20}$$

with (u, v, w) given by (7)–(8).

3.3. Regime II: Conduction dominated $Pe = O(1)$

Here we take $Pe = O(1)$ and, for reasons which will become clearer in Section 3.4, we write

$$\upsilon = \epsilon^2 \Upsilon, \qquad \lambda_a = \epsilon^2 \Lambda_a\,, \qquad \lambda_b = \epsilon^2 \Lambda_b\,,$$

with $\Upsilon, \Lambda_a, \Lambda_b = O(1)$ giving the fullest balance. By setting $\epsilon = 0$ in (17), we then obtain to leading order that

$$T = T(x,y,t), \tag{21}$$

an evolution equation for which can be derived either as a solvability condition for (17) at $O(\epsilon^2)$ or by applying (18) at leading order; either way we obtain

$$\begin{aligned} Pe\left(\frac{\partial}{\partial t}(hT) + \frac{\partial}{\partial x}(\bar{u}hT) + \frac{\partial}{\partial y}(\bar{v}hT)\right) &= \frac{\partial}{\partial x}\left(h\frac{\partial T}{\partial x}\right) + \frac{\partial}{\partial y}\left(h\frac{\partial T}{\partial y}\right) \\ &\quad - [\Lambda_a f_a(T;T_a) + \Lambda_b f_b(T;T_b)] + \Upsilon\int_0^h Q\,\mathrm{d}z. \end{aligned} \tag{22}$$

In view of (11), the left hand side of (22) can also be written as

$$Pe\,h\left(\frac{\partial T}{\partial t} + \bar{u}\frac{\partial T}{\partial x} + \bar{v}\frac{\partial T}{\partial y}\right). \tag{23}$$

Equations (21)–(22) provide our second thermal model, with (in view of (21)) the diffusivity (10) simplifying to the local form

$$D(h;T) = \frac{h^3}{3\mu(T)}\,.$$

Initial conditions on (22) can de deduced as follows. If

$$\text{at } t = 0 \qquad T = T_i(x,y,z) \tag{24}$$

applies on (17), then on the short (initial transient) timescale $t = O(\epsilon^2)$ the leading order balance is given by

$$\begin{aligned} &\epsilon^2 Pe \frac{\partial T}{\partial t} = \frac{\partial^2 T}{\partial z^2}, \\ &\text{at } z = 0,\ h(x,y,0) \qquad \frac{\partial T}{\partial z} = 0, \\ &\text{at } t = 0, \qquad\qquad T = T_i(x,y,z). \end{aligned} \tag{25}$$

The matching condition on (22) is then provided by the large-time behaviour of (25), giving the required initial condition

$$\text{at } t = 0 \qquad T = \bar{T}_i(x,y) \tag{26}$$

where

$$\bar{T}_i(x,y) = \frac{1}{h(x,y,0)} \int_0^{h(x,y,0)} T_i(x,y,z')\,\mathrm{d}z'. \tag{27}$$

3.4. Further simplifications

If $Pe_r \gg 1$ in (20) then, away from thermal boundary layers, the temperature field is simply advected, so if $T = T_i$ at $t = 0$ with T_i uniform then $T \sim T_i$ applies for all $t = O(1)$ and the problem is isothermal to leading order. On longer time scales the thermal boundary layers grow to occupy the whole fluid domain, with the conduction term re-entering at leading order. Of more significance is the limit $Pe_r \to 0$ in (20), in which case we have (after an initial transient)

$$\begin{aligned} &\frac{\partial^2 T}{\partial z^2} = -\upsilon Q, \\ &\text{at } z = 0 \qquad \frac{\partial T}{\partial z} = \lambda_b f_b(T;T_b), \\ &\text{at } z = h(x,y,t) \qquad \frac{\partial T}{\partial z} = -\lambda_a f_a(T;T_a), \end{aligned} \tag{28}$$

so for $\upsilon = 0$ (and constant T_a, T_b) it follows that

$$T = c(h) + d(h)z \tag{29}$$

where c and d are given by

$$d = \lambda_b f_b(c;T_b) = -\lambda_a f_a(c + dh\,;T_a). \tag{30}$$

Such cases with $\lambda_a, \lambda_b \to \infty$ are studied in more detail below (see Section 5.1).

With regard to regime II, we note that the scaling $\upsilon = \epsilon^2 \Upsilon$ implies that the internal heating is greatly increased in significance compared to regime I, in the sense that if $\upsilon \ll 1$ then it does not appear at leading order in the latter. This is a consequence of the slow ($\lambda_a, \lambda_b = O(\epsilon^2)$) transfer of heat across the fluid boundaries in regime II. If either or both Λ_a and Λ_b are large, then (22) simplifies significantly, with $T(x,y,t)$ being determined to leading order by

$$\Lambda_a f_a(T;T_a) + \Lambda_b f_b(T;T_b) = \Upsilon \int_0^h Q\,\mathrm{d}z, \tag{31}$$

corresponding to the small $\upsilon, \lambda_a, \lambda_b$ limit of (28) and providing the transition between the two regimes. In other words, when conduction dominates, the heat transfer rates must be small if the thermal problem is not to be very substantially constrained by the boundary conditions (as it

is in (31)). If Υ is large but Λ_a and Λ_b are not, Eq. (22) implies (not surprisingly) that high temperatures are attained within the fluid.

Finally, if $Pe \gg 1$ (but $Pe_r \ll 1$) we have from (22) and (23) that

$$\frac{\partial T}{\partial t} + \bar{u}\frac{\partial T}{\partial x} + \bar{v}\frac{\partial T}{\partial y} = 0 \tag{32}$$

to leading order, while if Pe, Λ_a, Λ_b and Υ are small, and there are no sources or sinks of fluid, it follows from (22) that

$$T = T(t) \tag{33}$$

to leading order with, from (19) or as a solvability condition on (22),

$$Pe\,\frac{\mathrm{d}}{\mathrm{d}t}(VT) = -S\left[\Lambda_a f_a(T;T_a) + \Lambda_b f_b(T;T_b)\right] + \Upsilon \int_{\Omega(t)} Q\,\mathrm{d}V \tag{34}$$

where $V = \int_{\Gamma_b(t)} h\,\mathrm{d}S$ is, to leading order, the volume of the fluid drop and $S(t) = \int_{\Gamma_b(t)} \mathrm{d}S$ is its horizontal cross-sectional area.

4. Numerical preliminaries

We first summarise the models to be solved in forms from which the appropriate radially symmetric systems are immediately apparent; here (and henceforth) we write

$$\boldsymbol{\nabla} = \left(\frac{\partial}{\partial x}, \frac{\partial}{\partial y}\right).$$

The flow problem has been reduced to the evolution equation

$$\frac{\partial h}{\partial t} = \boldsymbol{\nabla}\cdot(D(h;T)\boldsymbol{\nabla}h), \tag{35}$$

where D is given by (10) and (15); the velocity field is then determined to leading order by

$$\boldsymbol{u} = -\int_0^z \frac{(h-z')}{\mu}\,\mathrm{d}z'\,\boldsymbol{\nabla}h, \qquad w = \boldsymbol{\nabla}\cdot\left(\int_0^z \frac{(h-z')(z-z')}{\mu}\,\mathrm{d}z'\,\boldsymbol{\nabla}h\right), \tag{36}$$

$$\bar{\boldsymbol{u}} = -\frac{D(h;T)}{h}\boldsymbol{\nabla}h, \tag{37}$$

with $\boldsymbol{u} = (u, v)$, $\bar{\boldsymbol{u}} = (\bar{u}, \bar{v})$. The regime I energy equation is

$$Pe_r\left(\frac{\partial T}{\partial t} + \boldsymbol{u}\cdot\boldsymbol{\nabla}T + w\frac{\partial T}{\partial z}\right) = \frac{\partial^2 T}{\partial z^2} + vQ, \tag{38}$$

while in regime II we have

$$Pe\left(\frac{\partial}{\partial t}(hT) + \boldsymbol{\nabla}\cdot(\bar{\boldsymbol{u}}hT)\right) = \boldsymbol{\nabla}\cdot(h\boldsymbol{\nabla}T) - \left[\Lambda_a f_a(T;T_a) + \Lambda_b f_b(T;T_b)\right] + \Upsilon\int_0^h Q\,\mathrm{d}z \tag{39}$$

or, equivalently,

$$Pe\,\frac{\partial T}{\partial t} = \boldsymbol{\nabla}^2 T + \frac{(1+PeD(h;T))}{h}\boldsymbol{\nabla}h\cdot\boldsymbol{\nabla}T - \frac{1}{h}\left[\Lambda_a f_a(T;T_a) + \Lambda_b f_b(T;T_b)\right] + \frac{\Upsilon}{h}\int_0^h Q\,\mathrm{d}z\,. \tag{40}$$

Because of the degeneracy of D at $h = 0$ (this being most apparent in (15)), if the solution to (35) is initially compactly supported then it remains so with (requiring conservation of fluid at the contact line)

$$h = 0, \qquad D(h;T)\boldsymbol{\nabla}h\cdot\hat{\boldsymbol{\nu}} = 0 \quad \text{for} \quad \boldsymbol{x} \in \partial\Gamma_b(t) \tag{41}$$

where $\partial\Gamma_b(t)$ is the contact line at which the free surface meets the substrate, with $\hat{\boldsymbol{\nu}}$ denoting the unit vector on $z = 0$ in the outward normal direction to $\partial\Gamma_b(t)$; moreover, we have

$$V_n = \bar{\boldsymbol{u}} \cdot \hat{\boldsymbol{\nu}} \qquad \text{for} \quad \boldsymbol{x} \in \partial\Gamma_b(t) \tag{42}$$

where V_n is the outward normal velocity of $\partial\Gamma_b$, which expresses the rate at which the drop spreads. The corresponding result for (39) is the conservation of energy condition

$$h\boldsymbol{\nabla}T \cdot \hat{\boldsymbol{\nu}} = 0 \qquad \text{for} \quad \boldsymbol{x} \in \partial\Gamma_b(t), \tag{43}$$

which assumes there are no sources or sinks of heat at the contact line (an assumption we make throughout); because $h = 0$ on $\partial\Gamma_b$, expression (43) requires only that $\boldsymbol{\nabla}T \cdot \hat{\boldsymbol{\nu}}$ not be too singular there. Nevertheless, it can be shown that (43) in fact implies that

$$\boldsymbol{\nabla}T \cdot \hat{\boldsymbol{\nu}} = 0 \qquad \text{for} \quad \boldsymbol{x} \in \partial\Gamma_b(t); \tag{44}$$

indeed, defining X and Y to be outward normal and tangential coordinates along $\partial\Gamma_b$, we have as $X \to 0^-$ that

$$\begin{aligned} &T \sim T_c(Y,t), \qquad h \sim (9\mu(T_c)V_n)^{\frac{1}{3}}(-X)^{\frac{1}{3}}, \\ &\frac{\partial T}{\partial X} \sim -\frac{\Lambda_a f_a(T_c;T_a) + \Lambda_b f_b(T_c;T_a)}{(9\mu(T_c)V_n)^{\frac{1}{3}}}(-X)^{\frac{2}{3}}, \end{aligned} \tag{45}$$

for some function $T_c(Y,t)$ (the contact line temperature), with $V_n(Y,t) - \bar{\boldsymbol{u}} \cdot \hat{\boldsymbol{\nu}} = O(-X)$.

When discussing cylindrically symmetric cases, we introduce

$$u_r = \boldsymbol{u} \cdot \hat{\boldsymbol{r}}, \qquad \bar{u}_r = \bar{\boldsymbol{u}} \cdot \hat{\boldsymbol{r}} \tag{46}$$

where $\hat{\boldsymbol{r}}$ is the unit vector in the radial direction.

The model equations have been solved numerically subject to various initial and boundary conditions. We concentrate, in particular, on the problems that are two-dimensional (whereby, in particular, $h = h(x,t)$ and $v = 0$) or axisymmetric. For constant mass cases, the following initial profile and boundary conditions are applied:

$$\text{at } t = 0 \qquad h = (1 - r^2)_+, \tag{47}$$

$$\text{as } r \to \infty \qquad h \to 0; \tag{48}$$

the second of these is equivalent to the conditions

$$\text{at } r = s(t) \qquad h = D\frac{\partial h}{\partial r} = 0,$$

where $r = s(t)$ is the a priori unknown moving boundary (corresponding to $\partial\Gamma_b$), with $h = 0$ for $r \geq s(t)$; in practice (48) is applied numerically at the edge of the numerical domain. The spatial range in the following results usually denotes this boundary condition. Along the centreline we have the symmetry condition

$$\text{at } r = 0 \qquad \frac{\partial h}{\partial r} = 0. \tag{49}$$

In (47)–(49), r represents the Cartesian coordinate x in two-dimensional problems and the usual radial polar coordinate when the spreading is axisymmetric.

The inlet boundary condition for problems having an inflow from a line or a point source are given next. In the two-dimensional case, the injected fluid is assumed to be released along $x = 0$ at a rate $2\beta q_l t^{\beta-1}$, where q_l and β are positive constants. The global continuity equation is thus, modulo any initial mass present,

$$\int_0^{s(t)} h(x,t)\,\mathrm{d}x = q_l t^{\beta}. \tag{50}$$

This gives that

$$\text{at } x = 0^+ \qquad D\frac{\partial h}{\partial x} = -\beta q_l t^{\beta-1}\,. \tag{51}$$

Similarly, for a point source, whereby fluid is released from $r = 0$ at rate $q_p t^\beta$, we have

$$\text{at } r = 0 \qquad rD\frac{\partial h}{\partial r} = -\frac{\beta}{2\pi} q_p t^{\beta-1}\,. \tag{52}$$

The singularity at $r = 0$ is avoided by applying this condition at $r = \delta$, where $\delta = 0.01$ is typically adopted. To avoid problems initialising the numerical calculations, it is assumed that there is a small amount of mass present at the start, typically

$$\text{at } t = 0 \qquad h = 10(0.01 - r^2)_+\,. \tag{53}$$

To aid interpretation of the dynamics of the spreading viscous liquid, the stream function ψ will be used, where

$$u = \frac{\partial \psi}{\partial z}\,, \qquad w = -\frac{\partial \psi}{\partial x}\,, \tag{54}$$

so that

$$\psi = -\int_0^z \frac{(h - z')(z - z')}{\mu}\,\mathrm{d}z'\,\frac{\partial h}{\partial x}\,,$$

with, in particular, $\psi = h\bar{u}$ at $z = h$. Similarly, in the axisymmetric case use will be made of the Stokes stream function Ψ, where

$$u_r = -\frac{1}{r}\frac{\partial \Psi}{\partial z}\,, \qquad w = \frac{1}{r}\frac{\partial \Psi}{\partial r}\,, \tag{55}$$

giving

$$\Psi = r\int_0^z \frac{(h - z')(z - z')}{\mu}\,\mathrm{d}z'\,\frac{\partial h}{\partial r}\,,$$

whereby $\Psi = -rh\bar{u}_r$ at $z = h$. The stream functions are calculated numerically by the trapezium rule.

We now indicate through a number of examples some of the range of behaviour the above systems can exhibit; the examples chosen are illustrative rather than comprehensive, numerous other initial boundary value problems and parameter regimes also being of interest.

5. Results

5.1. Intermediate Peclet numbers

5.1.1. Hot and cold substrates

Section 5.1 is concerned with the limit $Pe_r \to 0$ of regime I, in which the temperature problem simplifies to (28); this can be viewed as an intermediate Peclet number formulation. We first consider one of the simplest possible problems, involving (28) with no internal heating ($\upsilon = 0$) and no mass input, with upper and lower surfaces of the spreading fluid held at (different) fixed temperatures (corresponding to taking $\lambda_a, \lambda_b \gg 1$). For the case $T_a < T_b$, we set $T_1 = T_a$ and $\Delta T = T_b - T_a$, giving dimensionless boundary conditions

$$\begin{aligned} &\text{at } z = 0 \qquad T = 1,\\ &\text{at } z = h \qquad T = 0. \end{aligned} \tag{56}$$

Hence the temperature field is given by

$$T = \frac{h-z}{h} = 1-\zeta, \tag{57}$$

which, from (15), gives

$$D(h) = D_H h^3,$$

where the constant D_H is given by

$$D_H = \int_0^1 \frac{(1-\zeta')^2}{\mu(1-\zeta')}\,\mathrm{d}\zeta' = \alpha^{-3}\left[e^{\alpha}(\alpha^2-2\alpha+2)-2\right]$$

when (16) holds. Thus

$$\frac{\partial h}{\partial t} = D_H \nabla\cdot(h^3\nabla h)\,. \tag{58}$$

In the converse case, when the substrate is cold, we take $\Delta T = T_a - T_b$ and $T_1 = T_b$, giving

$$T = z/h = \zeta,$$

so the factor D_H is replaced by D_C, where for (16) we have

$$D_C = \mathrm{e}^{\alpha} D_H(-\alpha) = \alpha^{-3}\left[2e^{\alpha} - (\alpha^2+2\alpha+2)\right]. \tag{59}$$

Solving (58) subject to (47), (48) and (49) using the NAG routine D03PGF correctly reproduces the isothermal model results of Huppert [9] when $D_H = 1/3$, corresponding to $\alpha = 0$.The evolution of the height profiles is illustrated in Fig. 2(a). The lens-shaped ('sloping shouldered') profiles in Fig. 2(a) are characteristic of the isothermal model and show very good agreement with the appropriate similarity solutions. The dependence of the hot substrate case upon D_H follows simply

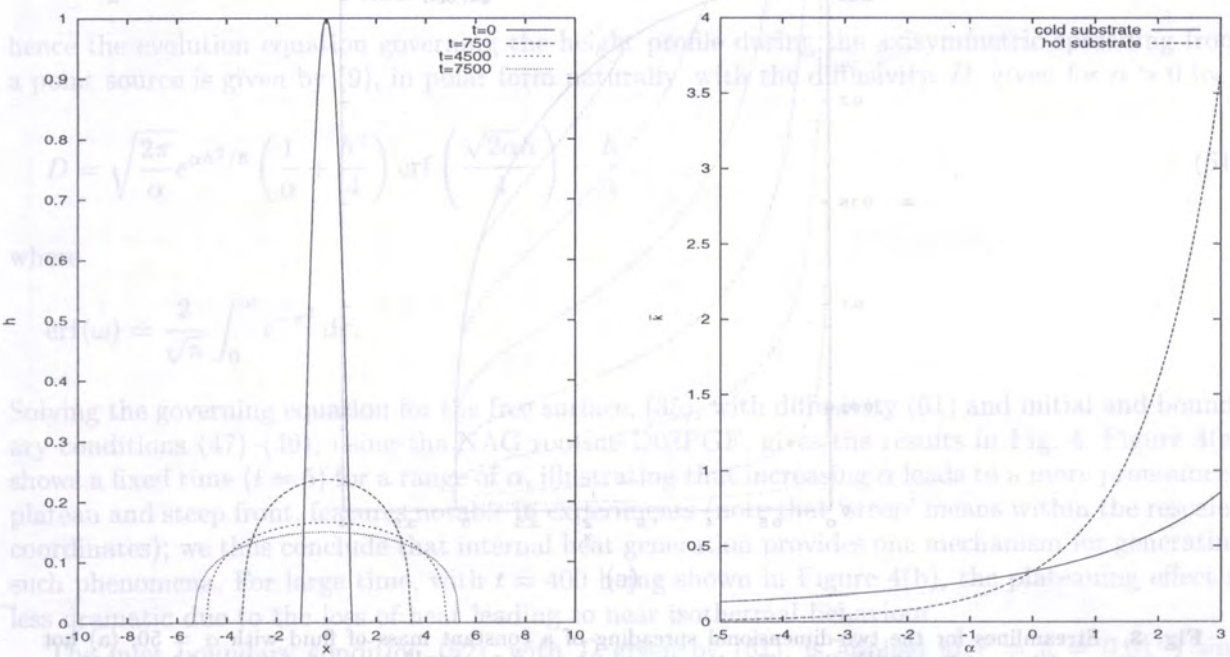

(a) (b)

Fig. 2. Two-dimensional spreading of a constant mass of fluid; (a) free surface profiles with $D_H = \frac{1}{3}$ and $t = 0,\ 750,\ 4500,\ 7500$; (b) D_H and D_C vs α

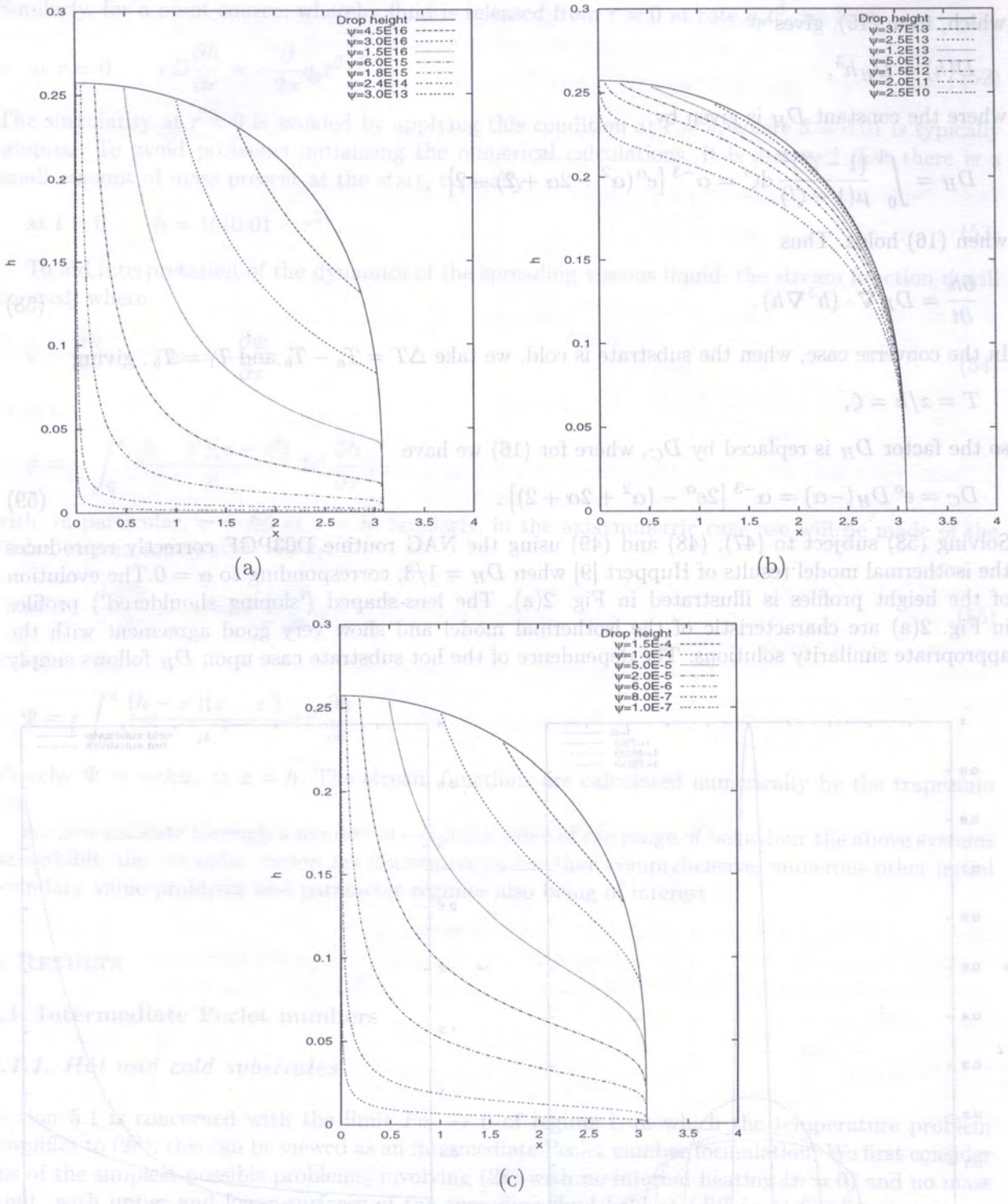

Fig. 3. Streamlines for the two-dimensional spreading of a constant mass of fluid with $\alpha = 50$; (a) hot substrate model, $t = 1.7 \times 10^{-18}$; (b) cold substrate model, $t = 2.0 \times 10^{-15}$ (c) isothermal model, $t = 500$

by scaling the time with $1/3D_H$ and that of the cold substrate case on D_C by scaling with $1/3D_C$. Consequently, the curves in Fig. 2(b) show that as α increases, the fluid spreads faster (as is to be expected). When $\alpha > 0$, we have $D_H > D_C$ and the fluid spreads faster over a hot substrate than over a cold one, as is to be expected since the viscosity near the plate, and hence the viscous drag, is smaller in the case of a hot substrate. This first example illustrates how a temperature field can influence the spreading dynamics, though not, in this special case, the droplet profile. It is very noteworthy that whenever T depends only on ζ and t, (35) can be mapped to the isothermal ($\mu = 1$) problem by introducing the new time variable

$$\tau = 3\int_0^t \int_0^1 \frac{(1-\zeta')^2}{\mu(T(\zeta', t'))}\, \mathrm{d}\zeta' \mathrm{d}t',$$

a result that follows immediately from (15). This correspondence is by no means obvious a priori; in particular, the streamlines differ between isothermal and non-isothermal cases, as shown in Fig. 3. The times in Figs. 3(a) and (b) are rescaled by $t = t_{\mathrm{iso}}/3D_H(\alpha)$ and $t = t_{\mathrm{iso}}/3D_C(\alpha)$ respectively, where t_{iso} is the value of time in Fig. 3(c); similarly the streamlines in Figs. 3(a) and (b) are rescaled by $\psi = 3D_H(\alpha)\psi_{\mathrm{iso}}$ and $\psi = 3D_C(\alpha)\psi_{\mathrm{iso}}$ respectively, where ψ_{iso} are the streamline values in Fig. 3(c). As to be expected, most of the flow in Figs. 3(a) and (b) occurs where the fluid is hottest and the viscosity therefore lowest.

5.1.2. Spreading with internal heat generation

We now retain the simplification that $\lambda_a, \lambda_b \to \infty$ in (28), but take $T_a = T_b$ and include a constant rate of internal heat generation throughout the fluid, showing simulations for the case of a point source of fluid. We set $vQ = 1$ and take $T_1 = T_a = T_b$ and $\Delta T = T_a$. The solution of (28) is then simply

$$T = \frac{1}{2}z(h-z); \tag{60}$$

hence the evolution equation governing the height profile during the axisymmetric spreading from a point source is given by (9), in polar form naturally, with the diffusivity, D, given for $\alpha > 0$ by

$$D = \sqrt{\frac{2\pi}{\alpha}} e^{\alpha h^2/8} \left(\frac{1}{\alpha} + \frac{h^2}{4}\right) \mathrm{erf}\left(\frac{\sqrt{2\alpha}h}{4}\right) - \frac{h}{\alpha}, \tag{61}$$

where

$$\mathrm{erf}(\omega) = \frac{2}{\sqrt{\pi}} \int_0^\omega e^{-\tau^2}\, \mathrm{d}\tau.$$

Solving the governing equation for the free surface, (35), with diffusivity (61) and initial and boundary conditions (47)–(49), using the NAG routine D03PGF, gives the results in Fig. 4. Figure 4(a) shows a fixed time ($t = 5$) for a range of α, illustrating that increasing α leads to a more pronounced plateau and steep front, features notable in experiments (note that 'steep' means within the rescaled coordinates); we thus conclude that internal heat generation provides one mechanism for generating such phenomena. For large time, with $t = 400$ being shown in Figure 4(b), the plateauing effect is less dramatic due to the loss of heat leading to near isothermal behaviour.

The inlet boundary condition (52), with D given by (61), is applied at $r = \delta = 0.01$. Using D03PGF again with the initial condition (53) results in Figs. 5 and 6, for $\alpha = 100$ and $\alpha = 340$, respectively. We again see that as α increases the steep flow front again becomes more pronounced. The streamline patterns show how the fluid flowing from the inlet ultimately feeds into the flow front.

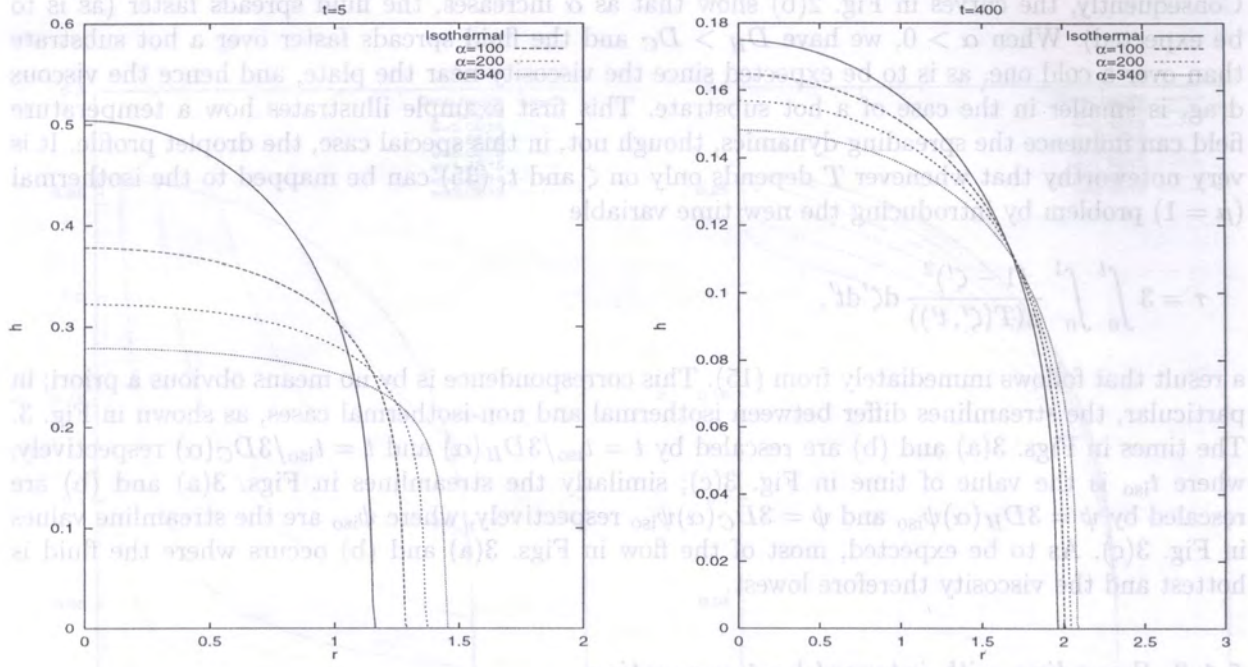

(a) (b)

Fig. 4. Axisymmetric spreading of a constant mass of fluid; (a) height profiles at $t = 5$: $\alpha = 0,\ 100,\ 200,\ 340$; (b) height profiles at $t = 400$: $\alpha = 0,\ 100,\ 200,\ 340$

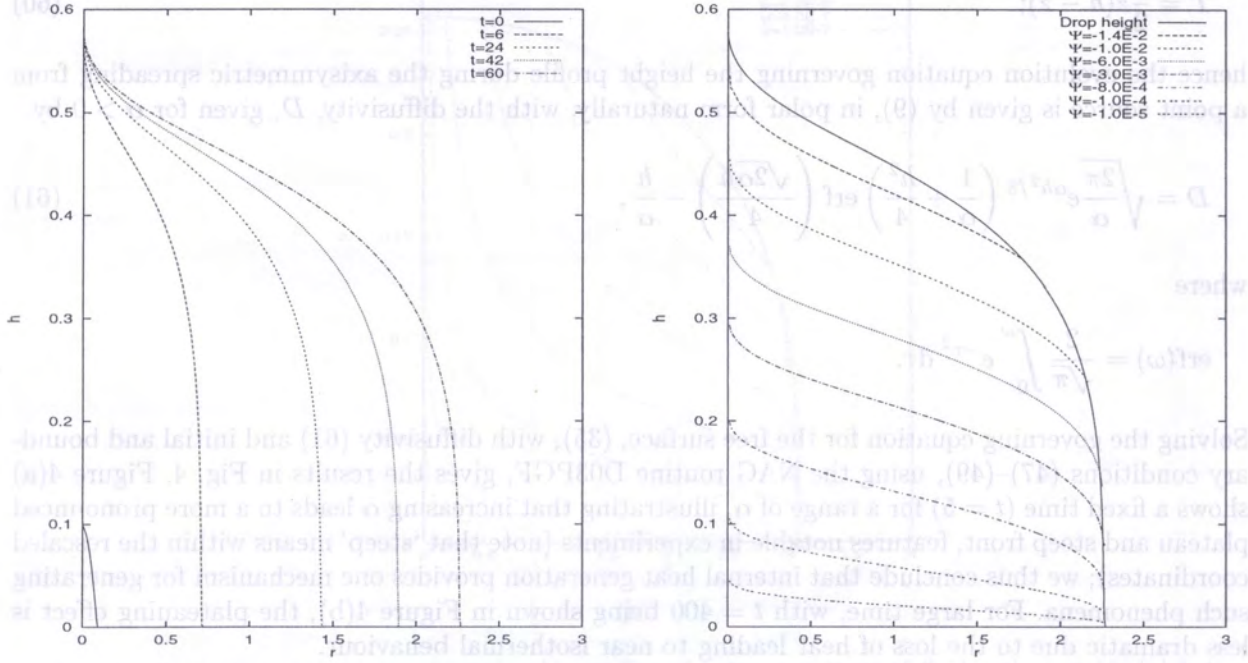

(a) (b)

Fig. 5. Axisymmetric spreading from a point source with $\alpha = 100$, $q_p = 0.1$ and $\beta = 1$; (a) evolution of the height profiles: $t = 0,\ 6,\ 24,\ 42,\ 60$; (b) streamlines at $t = 60$

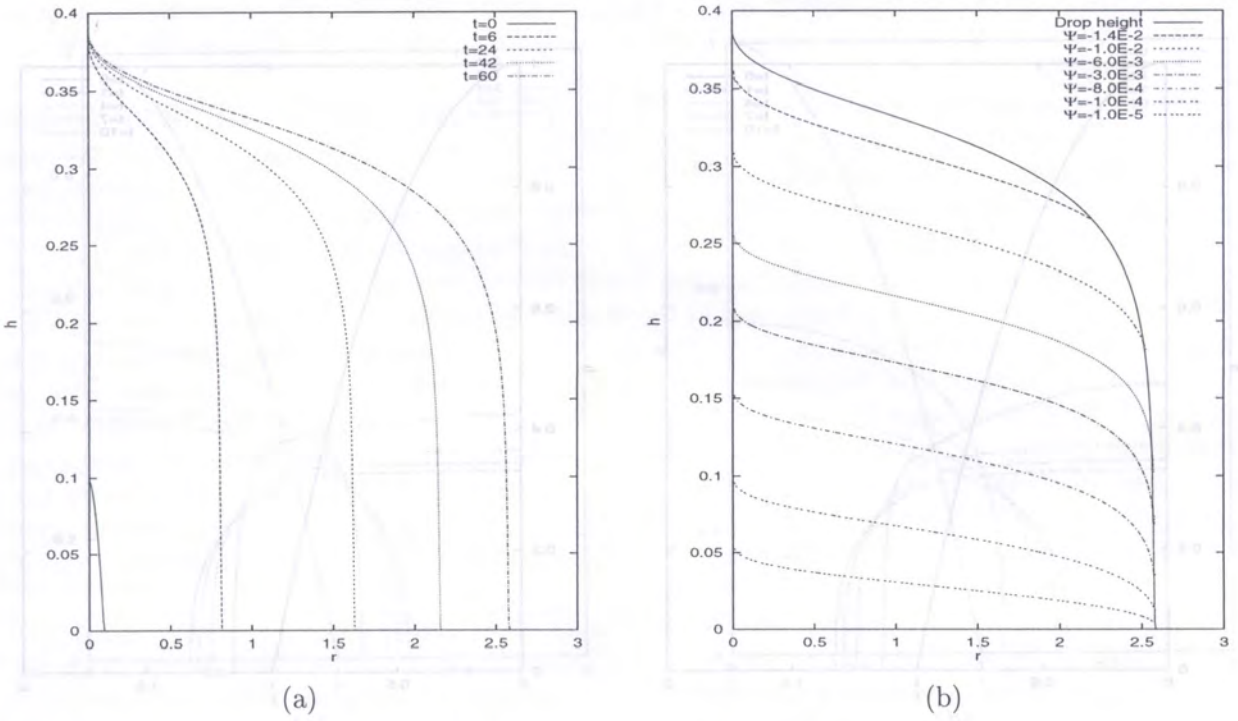

(a) (b)

Fig. 6. Axisymmetric spreading from a point source with $\alpha = 340$, $q_p = 0.1$ and $\beta = 1$; (a) evolution of height profiles: $t = 0,\ 6,\ 24,\ 42,\ 60$; (b) streamlines at $t = 60$

5.2. Large Peclet numbers: the conduction limited model

5.2.1. Numerical solutions

We now consider the axisymmetric spreading of a constant mass of fluid under regime I conditions. We assume that there is no internal heat generation ($v = 0$) and that $\lambda_a, \lambda_b \gg 1$, with $T_1 = T_a = T_b$ and $\Delta T = T_i - T_a$, where T_i denotes the (in this case dimensional) uniform initial temperature. To summarise, we now consider the coupled problem

$$\frac{\partial h}{\partial t} = \frac{1}{r}\frac{\partial}{\partial r}\left(rD\frac{\partial h}{\partial r}\right),$$

$$Pe_r\left(\frac{\partial T}{\partial t} + u_r\frac{\partial T}{\partial r} + w\frac{\partial T}{\partial z}\right) = \frac{\partial^2 T}{\partial z^2},$$

$$\text{at } t = 0 \qquad h = (1 - r^2)_+, \quad T = 1,$$

$$\text{at } z = 0,\ h(r,t) \qquad T = 0,$$

$$\text{at } r = 0 \qquad \frac{\partial T}{\partial r} = \frac{\partial h}{\partial r} = 0,$$

$$\text{as } r \to \infty \qquad h \to 0.$$

In the above,

$$u_r = -\int_0^z \frac{(h - z')}{\mu}\,\mathrm{d}z'\,\frac{\partial h}{\partial r}, \qquad w = \frac{1}{r}\frac{\partial}{\partial r}\left(r\int_0^z \frac{(h - z')(z - z')}{\mu}\,\mathrm{d}z'\,\frac{\partial h}{\partial r}\right),$$

$$D = \int_0^h \frac{(h - z')^2}{\mu}\,\mathrm{d}z',$$

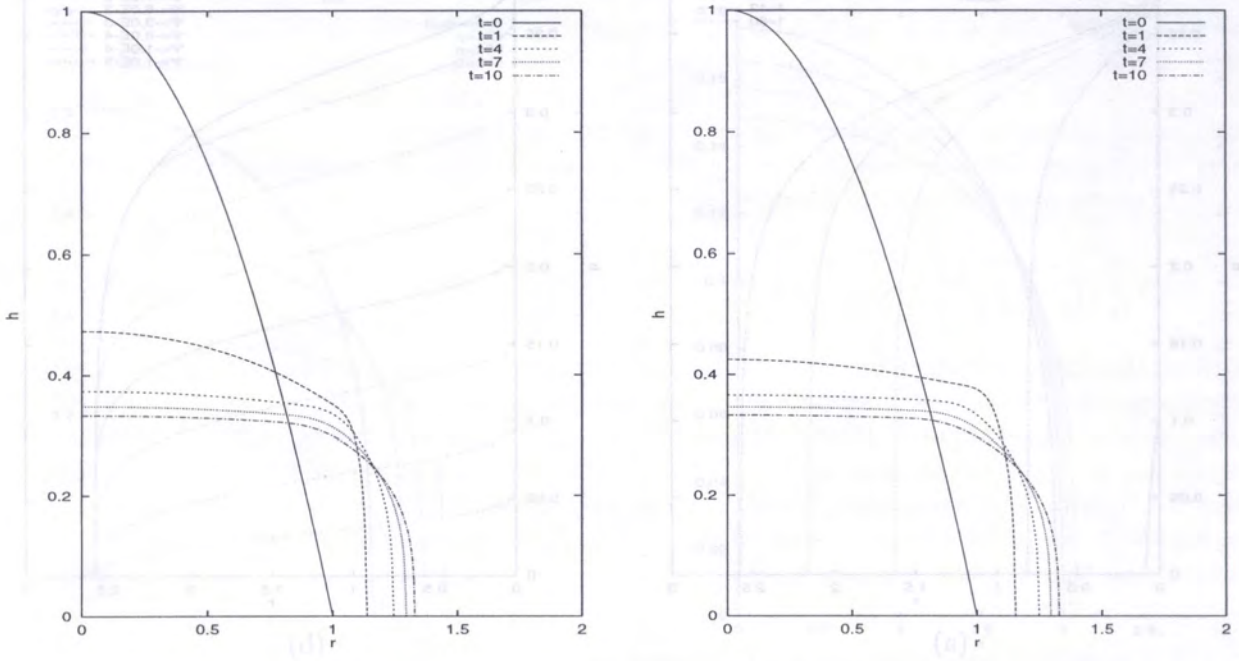

Fig. 7. Axisymmetric spreading of a constant mass when $Pe_r = 10^4$. Evolution of the height profiles: $t = 0,\ 1,\ 4,\ 7,\ 10$ when (a) $\alpha = 2$ and (b) $\alpha = 2.6$

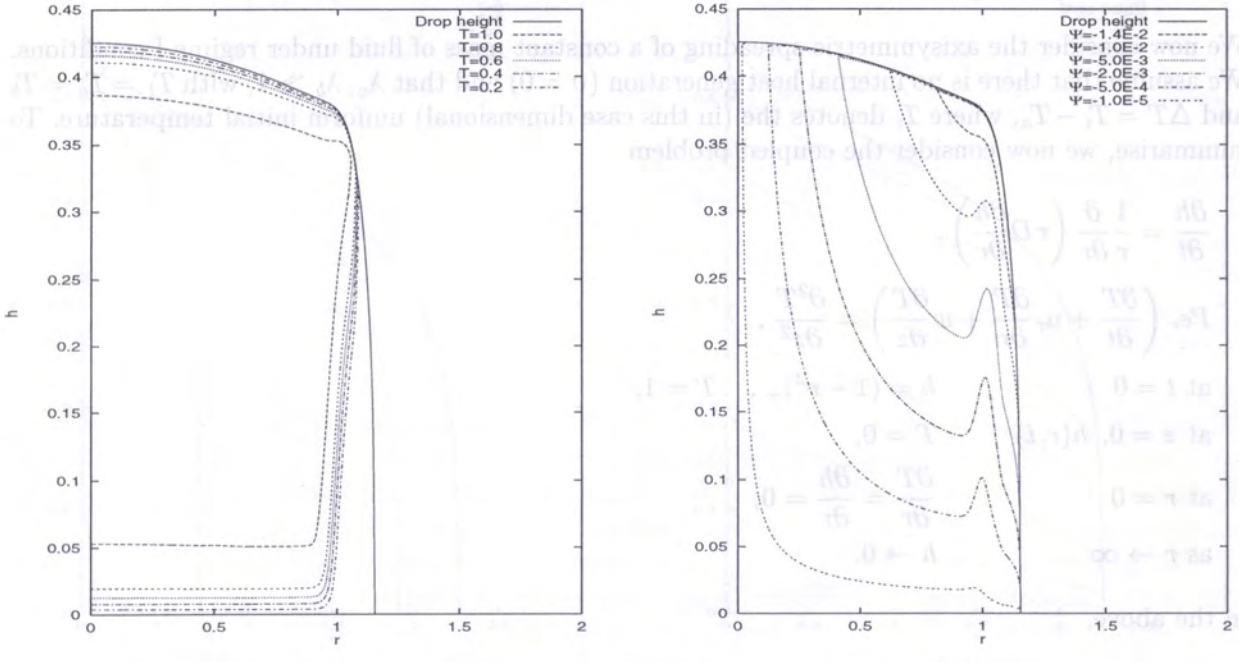

Fig. 8. Axisymmetric spreading of a constant mass when $Pe_r = 10^4$, $\alpha = 2.6$ and $t = 1$; (a) isotherms, (b) streamlines

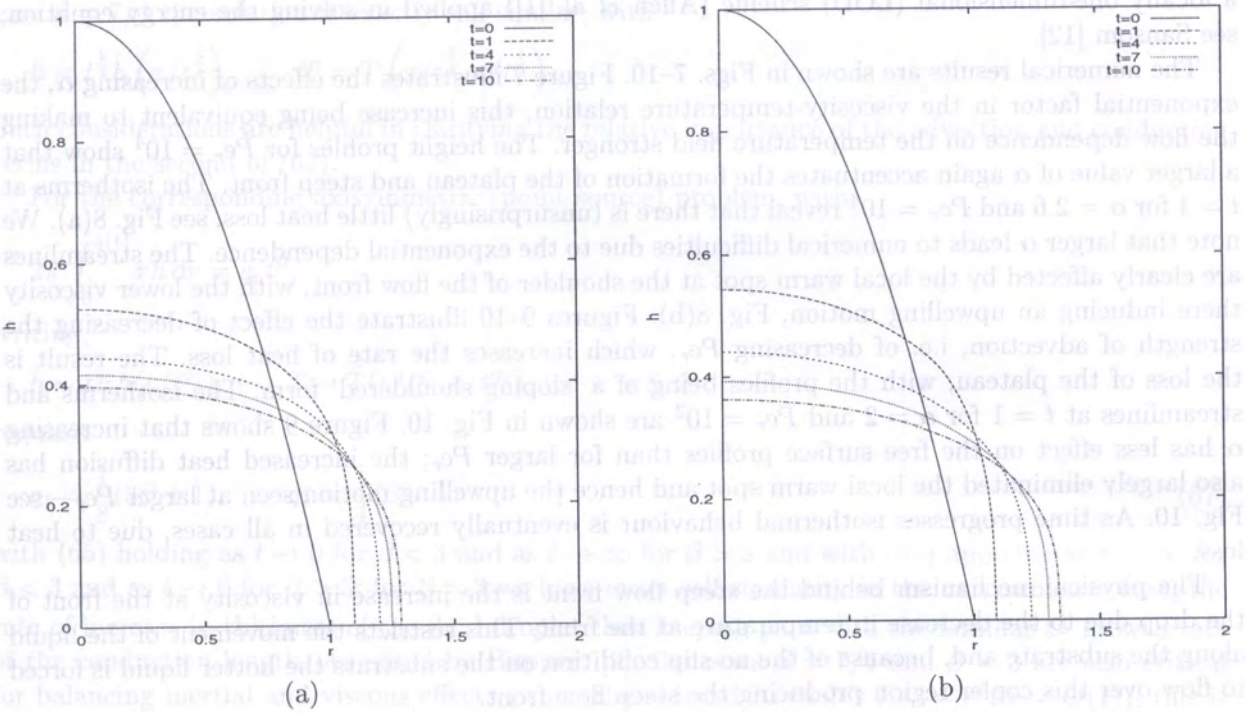

Fig. 9. Axisymmetric spreading of a constant mass when $Pe_r = 10^2$. Evolution of the height profiles: $t = 0,\ 1,\ 4,\ 7,\ 10$; (a) $\alpha = 2$ (b) $\alpha = 2.6$

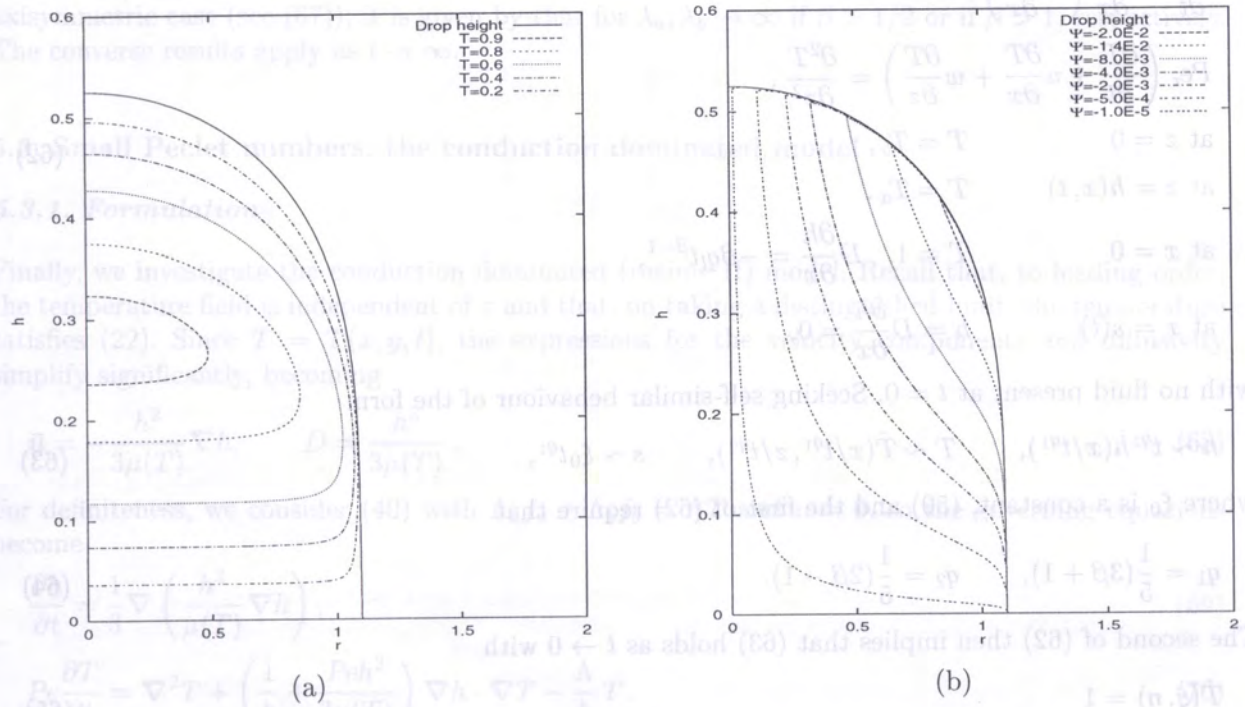

Fig. 10. Axisymmetric spreading of a constant mass when $Pe_r = 10^2$, $\alpha = 2$ and $t = 1$; (a) isotherms, (b) streamlines

with μ given by (16). The equations are solved using an implicit Crank–Nicolson method, with a locally one-dimensional (LOD) scheme (Allen *et al.* [1]) applied in solving the energy equation; see Sansom [12].

The numerical results are shown in Figs. 7–10. Figure 7 illustrates the effects of increasing α, the exponential factor in the viscosity-temperature relation, this increase being equivalent to making the flow dependence on the temperature field stronger. The height profiles for $Pe_r = 10^4$ show that a larger value of α again accentuates the formation of the plateau and steep front. The isotherms at $t = 1$ for $\alpha = 2.6$ and $Pe_r = 10^4$ reveal that there is (unsurprisingly) little heat loss; see Fig. 8(a). We note that larger α leads to numerical difficulties due to the exponential dependence. The streamlines are clearly affected by the local warm spot at the shoulder of the flow front, with the lower viscosity there inducing an upwelling motion, Fig. 8(b). Figures 9–10 illustrate the effect of decreasing the strength of advection, i.e. of decreasing Pe_r, which increases the rate of heat loss. The result is the loss of the plateau, with the profiles being of a 'sloping shouldered' form. The isotherms and streamlines at $t = 1$ for $\alpha = 2$ and $Pe_r = 10^2$ are shown in Fig. 10. Figure 9 shows that increasing α has less effect on the free surface profiles than for larger Pe_r; the increased heat diffusion has also largely eliminated the local warm spot and hence the upwelling motion seen at larger Pe_r – see Fig. 10. As time progresses isothermal behaviour is eventually recovered in all cases, due to heat loss.

The physical mechanism behind the steep flow front is the increase in viscosity at the front of the drop due to the decrease in temperature at the front. This restricts the movement of the liquid along the substrate and, because of the no-slip condition on the substrate the hotter liquid is forced to flow over this cooler region producing the steep flow front.

5.2.2. Self-similar behaviour

Here we set $v = 0$, $\lambda_a, \lambda_b \to \infty$ in (20) and consider the line source initial boundary value problem

$$\begin{aligned}
&\frac{\partial h}{\partial t} = \frac{\partial}{\partial x}\left(D\frac{\partial h}{\partial x}\right), \\
&Pe_r\left(\frac{\partial T}{\partial t} + u\frac{\partial T}{\partial x} + w\frac{\partial T}{\partial z}\right) = \frac{\partial^2 T}{\partial z^2}, \\
&\text{at } z = 0 \qquad T = T_b, \\
&\text{at } z = h(x,t) \qquad T = T_a, \\
&\text{at } x = 0 \qquad T = 1, \quad D\frac{\partial h}{\partial x} = -\beta q_1 t^{\beta-1}, \\
&\text{at } x = s(t) \qquad h = D\frac{\partial h}{\partial x} = 0,
\end{aligned} \tag{62}$$

with no fluid present at $t = 0$. Seeking self-similar behaviour of the form

$$h \sim t^{q_2}\hat{h}(x/t^{q_1}), \qquad T \sim \hat{T}(x/t^{q_1}, z/t^{q_2}), \qquad s \sim \xi_0 t^{q_1}, \tag{63}$$

where ξ_0 is a constant, (50) and the first of (62) require that

$$q_1 = \frac{1}{5}(3\beta + 1), \qquad q_2 = \frac{1}{5}(2\beta - 1). \tag{64}$$

The second of (62) then implies that (63) holds as $t \to 0$ with

$$\hat{T}(\xi, \eta) = 1 \tag{65}$$

(whereby the left-hand side dominates the second of (62)) for $\beta < 7/4$ and

$$\hat{T}(\xi, \eta) = T_b + (T_a - T_b)\eta/\hat{h}(\xi) \tag{66}$$

(with the right-hand side dominant) if $\beta > 7/4$; the reverse is the case as $t \to \infty$. In the special case $\beta = 7/4$ the solution is exactly self-similar, with

$$h = t^{\frac{1}{2}}\hat{h}\left(x/t^{\frac{5}{4}}\right), \qquad T = \hat{T}\left(x/t^{\frac{5}{4}}, z/t^{\frac{1}{2}}\right).$$

Such considerations are helpful in clarifying the relative importance of the advection and conduction terms in the second of (62).

For the corresponding axisymmetric (point source) problem, with

$$2\pi \int_0^{s(t)} rh \, \mathrm{d}r = q_p t^{\beta},$$

writing

$$h \sim t^{q_2}\hat{h}(r/t^{q_1}), \qquad T \sim \hat{T}(r/t^{q_1}, z/t^{q_2}), \qquad s \sim \xi_0 t^{q_1},$$

requires

$$q_1 = \frac{1}{8}(3\beta + 1), \qquad q_2 = \frac{1}{4}(\beta - 1) \tag{67}$$

with (65) holding as $t \to 0$ for $\beta < 3$ and as $t \to \infty$ for $\beta > 3$ and with (66) applying as $t \to \infty$ for $\beta < 3$ and as $t \to 0$ for $\beta > 3$; for $\beta = 3$ we have exact self-similarity in the axisymmetric case, the rate of increase in thickness of the fluid droplet then keeping pace with the familiar $t^{\frac{1}{2}}$ growth rate of the conduction length. As noted by Huppert [9], the cases $\beta = 7/4$ and $\beta = 3$ are also critical for balancing inertial and viscous effects (when the reduced Reynolds $Re_r = \epsilon^2 Re = O(1)$); this is to be expected since (38) with $v = 0$ shares the scaling properties of the corresponding momentum equations.

The above conclusions concerning the nature of time dependence also apply when one of the λ_a and λ_b tends to zero and the other tends to infinity (if both equal zero, one simply has $T = 1$). If $\lambda_a, \lambda_b = O(1)$ (so that the boundary conditions are those of (20)), then the small time behaviour corresponds to that for $\lambda_a, \lambda_b \to 0$ if $\beta < 1/2$ in two dimensions (see (64)) and if $\beta < 1$ in the axisymmetric case (see (67)); it is given by that for $\lambda_a, \lambda_b \to \infty$ if $\beta > 1/2$ or if $\beta > 1$, respectively. The converse results apply as $t \to \infty$.

5.3. Small Peclet numbers: the conduction dominated model

5.3.1. Formulation

Finally, we investigate the conduction dominated (regime II) model. Recall that, to leading order, the temperature field is independent of z and that, on taking a distinguished limit, the temperature satisfies (22). Since $T = T(x, y, t)$, the expressions for the velocity components and diffusivity simplify significantly, becoming

$$\bar{\boldsymbol{u}} = -\frac{h^2}{3\mu(T)}\boldsymbol{\nabla} h, \qquad D = \frac{h^3}{3\mu(T)}. \tag{68}$$

For definiteness, we consider (40) with $\Lambda_a f_a + \Lambda_b f_b = \Lambda T$ and $v = 0$, so the governing equations become

$$\frac{\partial h}{\partial t} = \frac{1}{3}\boldsymbol{\nabla}\left(\frac{h^3}{\mu(T)}\boldsymbol{\nabla} h\right), \tag{69}$$

$$Pe\frac{\partial T}{\partial t} = \boldsymbol{\nabla}^2 T + \left(\frac{1}{h} + \frac{Peh^2}{3\mu(T)}\right)\boldsymbol{\nabla} h \cdot \boldsymbol{\nabla} T - \frac{\Lambda}{h}T. \tag{70}$$

We consider two cases numerically, the first being flow from a line source, after which we illustrate the beginning of fingering in the spreading of a constant mass of fluid. The governing equations are again solved using numerical finite difference schemes, more details being given in Sansom [13].

5.3.2. Two-dimensional flow of constant mass

The problem is one-dimensional, and reads as follows:

$$\frac{\partial h}{\partial t} = \frac{1}{3}\frac{\partial}{\partial x}\left(\frac{h^3}{\mu(T)}\frac{\partial h}{\partial x}\right),$$

$$Pe\frac{\partial T}{\partial t} = \frac{\partial^2 T}{\partial x^2} + \left(\frac{1}{h} + \frac{Peh^2}{3\mu(T)}\right)\frac{\partial h}{\partial x}\frac{\partial T}{\partial x} - \frac{\Lambda}{h}T,$$

$$\text{at } t = 0 \qquad h = (1-x^2)_+ + 10^{-6}, \quad T = 1,$$

$$\text{as } x \to \infty \qquad h^3\frac{\partial h}{\partial x} = 0, \quad \frac{\partial T}{\partial x} = 0,$$

with $\mu(T) = \exp(-\alpha T)$. A prewetting film of thickness 10^{-6} has been included here to avoid the difficulty of tracking the sharp flow front, the temperature profiles being truncated at a droplet thickness of 10^{-4}. For $\alpha = 5.2$ (strong coupling between thermal and flow fields) and $Pe = 10^4$ (strong advection), the free surface profiles show the rapid development of a very steep flow front, which persists as the fluid spreads; see Fig. 11(a). The temperature profiles in Fig. 11(b) show little heat loss, as is to be expected, with the greatest heat transfer taking place near the flow front where the droplet is thinnest. The streamlines are illustrated in Fig. 12.

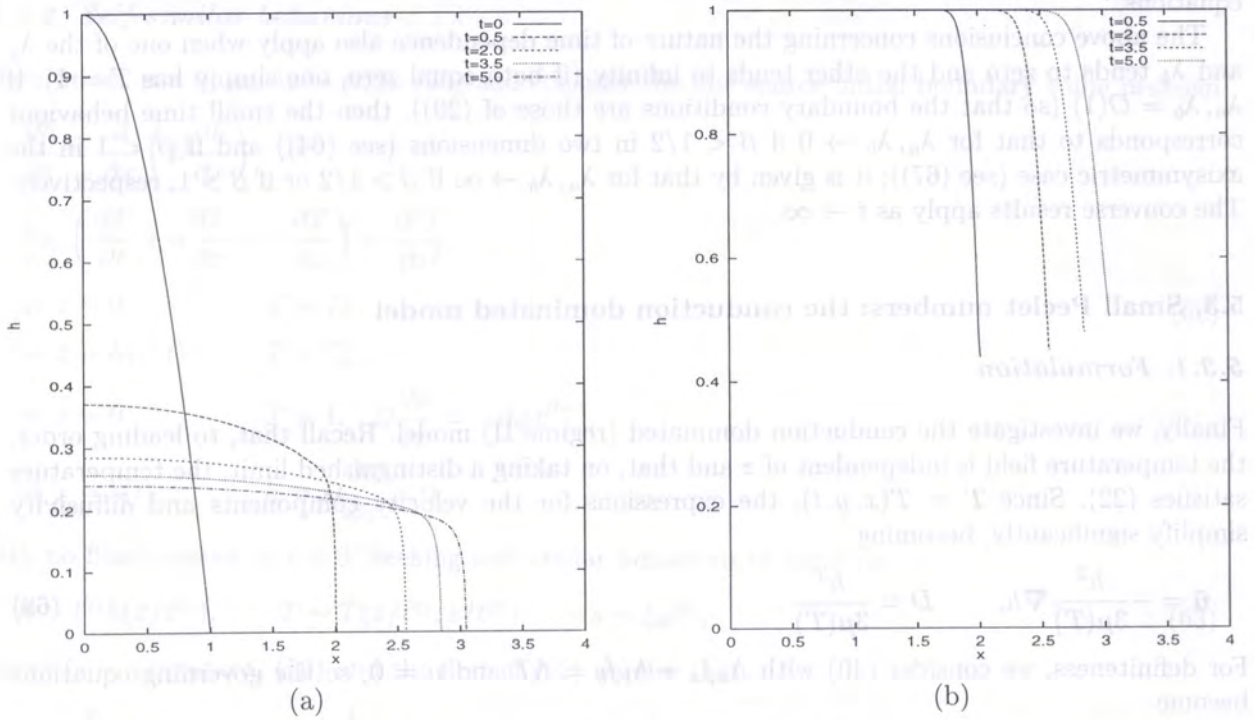

Fig. 11. Conduction dominated model: two-dimensional spreading from a line source when $Pe = 10^4$, $\Lambda = 0.5$ and $\alpha = 5.2$. Evolution of (a) height profiles and (b) temperature distributions: $t = 0,\ 0.5,\ 2.0,\ 3.5,\ 5.0$

Decreasing the Peclet number to unity gives the results in Fig. 13. The temperature profiles in Fig. 13(b) show a significant decrease in temperature and consequently displays an increase in viscosity. This is manifest in the height profiles shown in Fig. 13(a), where the spreading is retarded at later times.

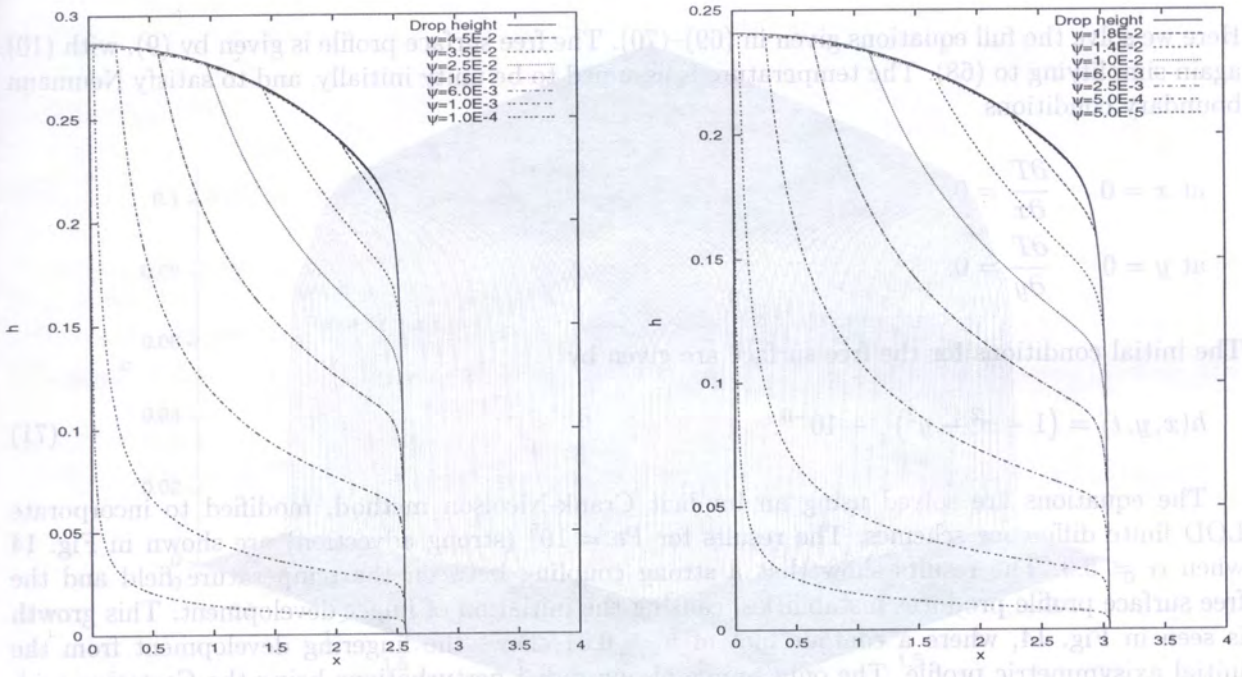

Fig. 12. Conduction dominated model: two-dimensional spreading of a constant mass of fluid when $Pe = 10^4$, $\Lambda = 0.5$ and $\alpha = 5.2$. Streamlines at (a) $t = 2$ (b) $t = 5$

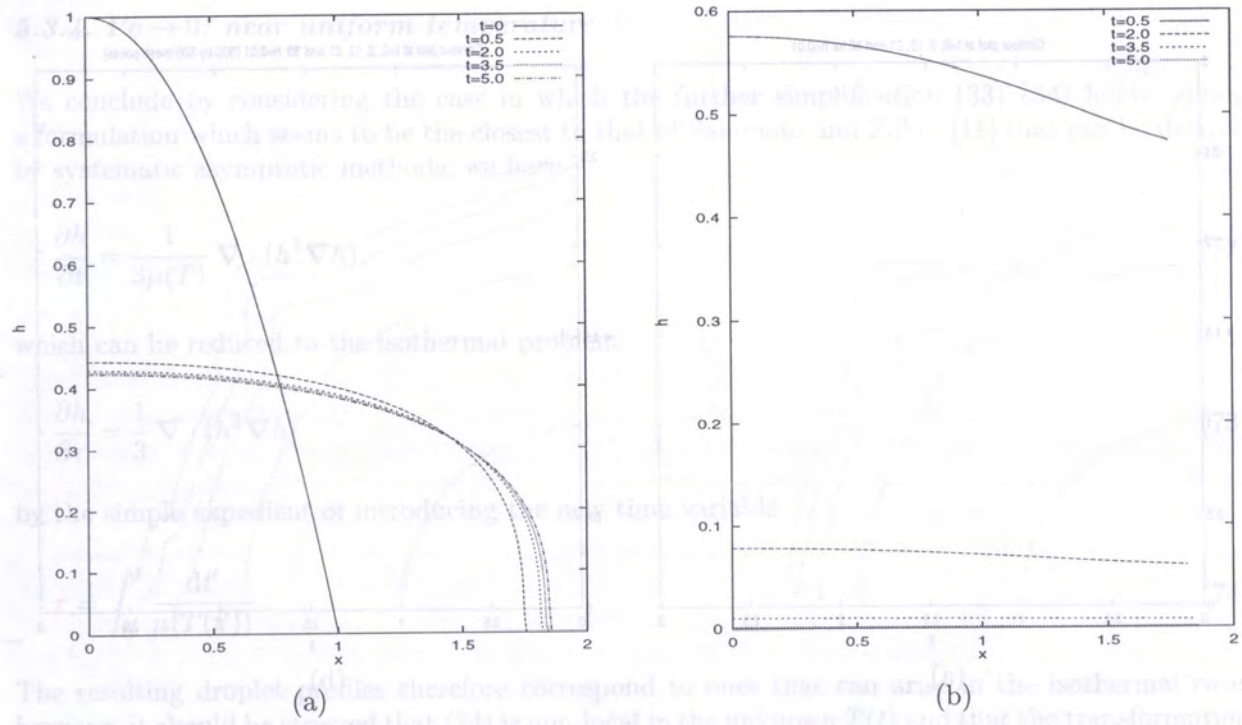

Fig. 13. Conduction dominated model: two-dimensional spreading of a constant mass of fluid when $Pe = 1$, $\Lambda = 0.5$ and $\alpha = 5.2$. Evolution of (a) height profiles and (b) temperature distributions: $t = 0,\ 0.5,\ 2.0,\ 3.5,\ 5.0$

5.3.3. Near radial spreading of a fluid of constant mass

Here we solve the full equations given in (69)–(70). The free surface profile is given by (9), with (10) again simplifying to (68). The temperature is assumed to be unity initially, and to satisfy Neumann boundary conditions

$$\text{at } x = 0 \qquad \frac{\partial T}{\partial x} = 0,$$

$$\text{at } y = 0 \qquad \frac{\partial T}{\partial y} = 0.$$

The initial conditions for the free surface are given by

$$h(x, y, t) = \left(1 - x^2 - y^2\right)_+ + 10^{-6}. \tag{71}$$

The equations are solved using an implicit Crank-Nicolson method, modified to incorporate LOD finite difference schemes. The results for $Pe = 10^5$ (strong advection) are shown in Fig. 14 when $\alpha = 5.9$. The results show that a strong coupling between the temperature field and the free surface profile produces instabilities, causing the initiation of finger development. This growth is seen in Fig. 14, where a contour plot of $h = 0.01$ shows the fingering development from the initial axisymmetric profile. The only source of non-radial perturbations being the Cartesian grid, where introducing more mesh point introduces more instabilities. The free surface profile in Fig. 15 shows the development of a steep flow front followed by a plateau as in the two-dimensional and axisymmetric results as well as the instabilities. Here we have hotter fluid pushing against the cooler fluid near to the contact line, so we have a situation in which less viscous fluid is displacing fluid that is more viscous. This is the physical basis on which Snyder and Tait [14] postulated that the instability is analogous to the Saffman–Taylor fingering [10].

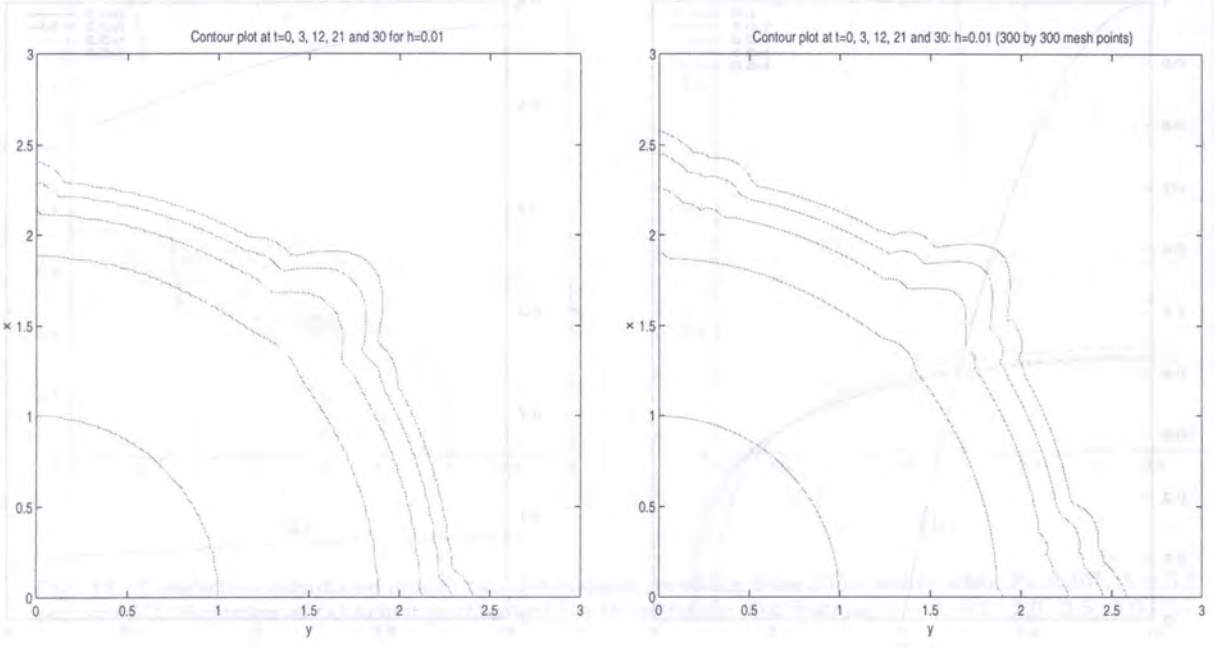

(a) (b)

Fig. 14. Conduction dominated model: three-dimensions when $Pe = 10^5$, $\alpha = 5.9$ and $\Lambda = 0.5$. Contour plots of $h = 0.01$ at $t = 3, 12, 21$ and 30; (a) 120 by 120 mesh points, (b) 300 by 300 mesh points

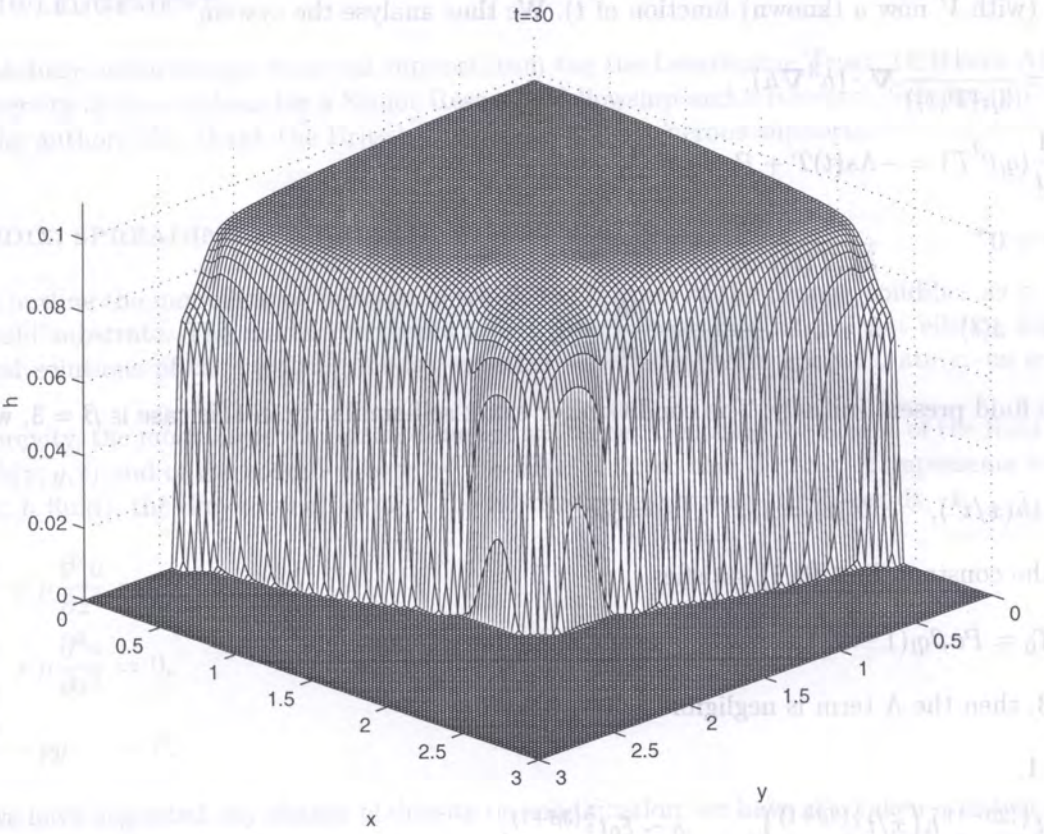

Fig. 15. Conduction dominated model: three-dimensions when $Pe = 10^5$, $\alpha = 5.9$ and $\Lambda = 0.5$. Free surface profile at $t = 30$ $h = 0.01$ at $t = 30$ with 120 by 120 mesh points

5.3.4. $Pe \to 0$: near uniform temperature

We conclude by considering the case in which the further simplification (33)–(34) holds, giving a formulation which seems to be the closest to that of Sakimoto and Zuber [11] that can be derived by systematic asymptotic methods; we have

$$\frac{\partial h}{\partial t} = \frac{1}{3\mu(T)} \nabla \cdot (h^3 \nabla h), \tag{72}$$

which can be reduced to the isothermal problem

$$\frac{\partial h}{\partial \tau} = \frac{1}{3} \nabla \cdot (h^3 \nabla h) \tag{73}$$

by the simple expedient of introducing the new time variable

$$\tau = \int_0^t \frac{\mathrm{d}t'}{\mu(T(t'))}. \tag{74}$$

The resulting droplet profiles therefore correspond to ones that can arise in the isothermal case; however, it should be stressed that (74) is non-local in the unknown $T(t)$ and that the transformation may be unhelpful when t appears explicitly in the boundary conditions. As an example, we discuss a line source case, first noting that if fluid at temperature $T = 1$ is being injected at a rate $q(t)$, then the quantity $\epsilon^2 Pe\, q(t)$ needs to be added to the right-hand side of (19) and $Pe\, q(t)$ to that

of (34) (with V now a (known) function of t). We thus analyse the system

$$\begin{aligned}
&\frac{\partial h}{\partial t} = \frac{1}{3\mu(T(t))}\,\boldsymbol{\nabla}\cdot(h^3\boldsymbol{\nabla}h),\\
&Pe\frac{\mathrm{d}}{\mathrm{d}t}(q_l t^\beta T) = -\Lambda s(t)T + Pe\,\beta q_l t^{\beta-1},\\
&\text{at } x=0^+ \qquad \frac{h^3}{3\mu(T(t))}\frac{\partial h}{\partial x} = -\beta q_l t^{\beta-1},\\
&\text{at } x=s(t) \qquad h=0,\quad \frac{h^3}{3\mu(T(t))}\frac{\partial h}{\partial x} = 0,
\end{aligned} \tag{75}$$

with no fluid present initially. The condition for exact self-similarity in this case is $\beta = 3$, when one has

$$h = t\hat{h}(x/t^2), \qquad T(t) = T_0, \qquad s = \xi_0 t^2,$$

where the constant $T_0 \in (0,1)$ satisfies

$$\Lambda\xi_0 T_0 = Pe\,\beta q_l(1-T_0).$$

If $\beta < 3$, then the Λ term is negligible as $t \to 0$, giving

$$T \sim 1, \tag{76}$$

$$h \sim t^{\frac{1}{5}(2\beta-1)}\,\hat{h}\left(x/t^{\frac{1}{5}(3\beta+1)}\right), \qquad s \sim \xi_0 t^{\frac{1}{5}(3\beta+1)}, \tag{77}$$

reproducing the Barenblatt self-similar forms; conversely, (76)–(77) hold as $t \to \infty$ for $\beta > 3$. The other relevant asymptotic balance occurs when the left-hand side of the second of (75) is negligible, giving (77), with $\mu(T)$ replaced by $\mu(0)$ in the first of (75), together with

$$T \sim \frac{Pe\,\beta q_l}{\Lambda\xi_0}\,t^{\frac{2}{5}(\beta-3)}; \tag{78}$$

this balance holds as $t \to \infty$ for $\beta < 3$ and as $t \to 0$ for $\beta > 3$.

6. Conclusions

In this paper we have studied the flow over a horizontal substrate of gravity currents with temperature dependent viscosity for cases in which the horizontal extent of the current greatly exceeds its thickness. The two distinguished limits have been identified and sample numerical solutions given. The regime I (conduction limited) case involves no reduction of dimensionality in the thermal problem and hence provides the most computationally time-consuming examples. By contrast, for regime II (in which, unlike regime I, the temperature is to leading order independent of z) the formulations of both the flow and the thermal problems involve only the horizontal co-ordinates.

A number of relatively straightforward extensions to the analysis suggest themselves, such as generalising to allow for a temperature dependent thermal conductivity $k(T)$ or incorporating viscous dissipation into the heat source term Q. The inclusion of inertial effects through an $O(1)$ reduced Reynolds number is less straight forward, since the flow problem does not then benefit from a reduction in dimensionality. Some of the approaches outlined above remain applicable, however, including the use of self-similar solutions to characterise the relative contributions of the various effects; moreover, the derivation of the thermal models given in Section 2 carries over essentially unchanged.

ACKNOWLEDGEMENTS

JRK gratefully acknowledges financial support from the the Leverhulme Trust; DSR and AS thank the University of Nottingham for a Senior Research Fellowship and a Research Scholarship, respectively; the authors also thank the British Council for their generous support.

APPENDIX: SPREADING WITH BASAL SOLIDIFICATION

Here we outline the modelling of the case in which the bottom of the droplet solidifies as it spreads over a cold substrate. The model represents a first step in including latent heat effects. Extensive numerical solutions of the resulting model, together with asymptotic analysis, are given in Crossley [4].

For brevity, the model is developed in dimensional terms. Denoting the height of the fluid droplet by $z = h(x, y, t)$ and of the solidified base by $z = H(x, y, t)$ (so that $0 < z < H$ represents solid and $H < z < h$ fluid), the dimensional form of the lubrication equations (3)–(5) reads

$$-\frac{\partial p}{\partial x} + \mu \frac{\partial^2 u}{\partial z^2} = 0, \tag{79}$$

$$-\frac{\partial p}{\partial y} + \mu \frac{\partial^2 v}{\partial z^2} = 0, \tag{80}$$

$$-\frac{\partial p}{\partial z} - \rho g \quad = 0, \tag{81}$$

where we have neglected any change of density on solidification; we have also taken μ to be constant, though the formulation readily generalises to incorporate a temperature dependent viscosity. On $z = H$ we have $u = v = w = 0$, while on $z = h$ we apply the conditions from (6). It follows using incompressibility that the kinematic condition on $y = h$ can now be written as

$$\frac{\partial h}{\partial t} + \frac{\partial}{\partial x}\int_H^h u \, \mathrm{d}z + \frac{\partial}{\partial y}\int_H^h v \, \mathrm{d}z = 0. \tag{82}$$

Since

$$(u, v) = -\frac{\rho g}{2\mu}(z - H)(2h - H - z)\left(\frac{\partial h}{\partial x}, \frac{\partial h}{\partial y}\right), \tag{83}$$

Eq. (82) implies that

$$\frac{\partial h}{\partial t} = \frac{\rho g}{3\mu}\left[\frac{\partial}{\partial x}\left((h - H)^3 \frac{\partial h}{\partial x}\right) + \frac{\partial}{\partial y}\left((h - H)^3 \frac{\partial h}{\partial y}\right)\right]. \tag{84}$$

To close the system we require an evolution equation for $H(x, y, t)$ and to obtain this we assume large latent heat of solidification, in which case the leading order temperature problem for a thin droplet is simply

$$\frac{\partial^2 T}{\partial z^2} = 0 \qquad \text{in } 0 < z < H \text{ and } H < z < h, \tag{85}$$

$$\text{at } z = 0 \qquad k_s \frac{\partial T}{\partial z} = \lambda_b f_b(T; T_b), \tag{86}$$

$$\text{at } z = H \qquad k_s \left.\frac{\partial T}{\partial z}\right|_{z=H^-} - k_l \left.\frac{\partial T}{\partial z}\right|_{z=H^+} = L\rho \frac{\partial H}{\partial t}, \qquad T = T_m, \tag{87}$$

$$\text{at } z = h \qquad k_l \frac{\partial T}{\partial z} = -\lambda_a f_a(T; T_a) \tag{88}$$

where k_s and k_l are the thermal conductivities in the solid and liquid, respectively, L is the latent heat, ρ the density and T_m the melting temperature. $T_b < T_m$ is the substrate temperature and T_a the ambient temperature (we assume this to be sufficiently high (or the heat transfer at $z = h$ to be sufficiently slow) that all the solidification occurs from the base upwards); the function $\lambda_b f_b(T; T_b)$ is the rate of heat transfer between solidified melt and substrate, with $f_b(T_b; T_b) = 0$ and $f_b(T; T_b) > 0$ for $T > T_b$, while $\lambda_a f_a(T; T_a)$ is that between the melt and the surroundings, with $f_a(T_a; T_a) = 0$ and $f_a(T; T_a) < 0$ for $T < T_a$.

Writing

$$T = T_m - a_s(x, y, t)(H - z) \qquad 0 < z < H,$$

and

$$T = T_m + a_l(x, y, t)(z - H) \qquad H < z < h,$$

the unknowns a_s, a_l and H are given by

$$k_s a_s = \lambda_b f_b(T_m - a_s H\,;\, T_b), \tag{89}$$

$$k_l a_l = -\lambda_a f_a(T_m + a_l(h - H)\,;\, T_a) \tag{90}$$

$$k_s a_s - k_l a_l = L\rho \frac{\partial H}{\partial t}\,, \tag{91}$$

which, with (84), provide a closed system. A particularly simple case is when λ_b is sufficiently large and λ_a sufficiently small that the conditions in (86)–(88) at $z = 0$ and $z = h$ can be simplified to

$$\text{at } z = 0 \qquad T = T_b\,, \tag{92}$$

$$\text{at } z = h \qquad \frac{\partial T}{\partial z} = 0, \tag{93}$$

in which case we have $a_s = (T_m - T_b)/H$, $a_l = 0$ and we arrive at (84) and

$$L\rho H \frac{\partial H}{\partial t} = k_s(T_m - T_b) \tag{94}$$

as the evolutionary system for h and H.

References

[1] M.B. Allen, I. Herrera, and G.F. Pinder. *Numerical modelling in science and engineering.* John Wiley and Sons, 1988.

[2] G.I. Barenblatt. On some unsteady motions of a liquid or gas in a porous medium. *Prikl. Mat. Mech.*, **16**: 67–78, 1952.

[3] D. Bercovici. A theoretical model of cooling viscous gravity currents with temperature-dependent viscosity. *Geophys. Res. Lett.*, **21**: 1177–1180, 1994.

[4] J.A. Crossley. *The spreading of solidifying melts.* Third year BSc Project, University of Nottingham, 1998.

[5] J.H. Fink and R.W. Griffiths. Radial spreading of viscous-gravity currents with solidifying crust. *J. Fluid Mech.*, **221**: 485–509, 1990.

[6] J.H. Fink and R.W. Griffiths. A laboratory analog study of the surface morphology of lava flows extruded from point and line sources. *J. Volc. Geotherm. Res.*, **54**: 19–32, 1992.

[7] R.W. Griffiths and J.H. Fink. Solidifying Bingham extrusions: a model for the growth of silicic lava domes. *J. Fluid Mech.*, **347**: 13–36, 1997.

[8] E. Hallot, M.V. Stasiuk, S.R. Allan, D.S. Riley, and R.S.J. Sparks. *Experiments on solidification of viscous gravity currents.* Nuclear Electric Report, 1994.

[9] H.E. Huppert. The propagation of two-dimensional and axisymmetric viscous gravity currents over a rigid horizontal surface. *J. Fluid Mech.*, **121**: 43–48, 1982.

[10] P.G. Saffman and G.I. Taylor. The penetration of a fluid into a porous medium or Hele-Shaw cell containing a more viscous liquid. *Proc. R. Soc. Lond. A*, **245**: 312–329, 1958.

[11] S.E.H. Sakimoto and M.T. Zuber. The spreading of variable-viscosity axisymmetric radial gravity currents: applications to the emplacement of Venusian 'pancake' domes. *J. Fluid Mech.*, **301**: 65–77, 1995.

[12] A. Sansom. *The spreading of a temperature-dependent viscous drop.* Qualifying dissertation, University of Nottingham, 1997.

[13] A. Sansom. *Gravity currents with temperature-dependent viscosity.* PhD Thesis, University of Nottingham, 1999.

[14] D. Snyder and S. Tait. A flow-front instability in viscous gravity currents. *J. Fluid Mech.*, **369**: 1–21, 1998.

[15] M.V. Stasiuk, C. Jaupart, and R.S.J. Sparks. Influence of cooling on lava-flow dynamics. *J. Geol.*, **21**: 335–338, 1993.